The Astrophysical Journal Supplement Series, 268:2 (17pp), 2023 September https://doi.org/10.3847/1538-4365/acdb6b

Precise Transit Photometry Using TESS: Updated Physical Properties for 28 Exoplanets around Bright Stars

Suman Saha[1,2]
[1] Indian Institute of Astrophysics, II Block, Koramangala, Bengaluru, India; suman.saha@iiap.res.in
[2] Pondicherry University, R.V. Nagar, Kalapet, Puducherry, India
Received 2023 February 28; revised 2023 May 26; accepted 2023 June 2; published 2023 August 17

Abstract

The Transiting Exoplanet Survey Satellite (TESS) follow-up of a large number of known transiting exoplanets provides a unique opportunity to study their physical properties more precisely. Being a space-based telescope, the TESS observations are devoid of any noise component resulting from the interference of Earth's atmosphere. TESS also provides a greater probability to observe subsequent transit events owing to its longer uninterrupted time-series observations compared to ground-based telescopes. For the exoplanets around bright host stars in particular, TESS time-series observations provide high signal-to-noise ratio (S/N) lightcurves, which can be used for higher-precision studies for these exoplanets. In this work, I have studied the TESS transit photometric follow-up observations of 28 exoplanets around bright stars with $V_{\rm mag} \leqslant 10$. The already high-S/N lightcurves from TESS have been further processed with a critical noise-treatment algorithm, using the wavelet-denoising and the Gaussian-process regression techniques, to effectively reduce the noise components, both correlated and uncorrelated in time, which were then used to estimate the physical properties of these exoplanets. The study has resulted in very precise values for the physical properties of the target exoplanets, with the improvements in precision being significant for most of the cases compared to the previous studies. Also, since a comparatively large number of transit lightcurves from TESS observations were used to estimate these physical properties for each of the target exoplanets, which removes any bias due to the lack of sufficient data sets, these updated physical properties can be considered extremely accurate and reliable for future studies.

Unified Astronomy Thesaurus concepts: Transit photometry (1709); Exoplanets (498); Hot Jupiters (753); Gaussian Processes regression (1930); Wavelet analysis (1918)

1. Introduction

The Transiting Exoplanet Survey Satellite (TESS; Ricker et al. 2015) is a survey telescope for discovering new exoplanets around nearby bright stars. Over the span of this entire survey, TESS will cover a large portion (>90%) of the sky. This also means that TESS automatically does follow-up observations of many of the previously known exoplanets. Most of the previously known exoplanets discovered by ground-based survey missions have so far only been studied using the observations from small (sub–2 m class) ground-based telescopes, which are both affected by the noise components from the interference of Earth's atmosphere and limited by the reduced signal-to-noise ratio (S/N) in the observed lightcurves. This has resulted in large uncertainties in the currently known physical properties of these exoplanets. However, TESS, being a space-based instrument, provides observations not affected by the Earth's atmosphere. For the nearby bright stars in particular, the TESS lightcurves have reasonably high S/N. This gives a unique opportunity to conduct follow-up studies of the transiting exoplanets around nearby bright stars, which can give a more precise and accurate estimation of their physical properties.

In this work, I have studied the transit photometric follow-up observations of 28 exoplanets around bright stars with $V_{\rm mag} \leqslant 10$ from TESS, to estimate their physical properties with greater accuracy and precision compared to the previous studies. Being very bright stars, the TESS photometric lightcurves obtained for these targets are expected to have high S/N. Also, I have found that for most of these targets, the currently known parameter values estimated in previous studies have large uncertainties, as they were previously estimated from ground-based transit observations. This is motivation for a transit follow-up study using TESS observations, which could provide a better estimation of these physical properties.

One of the major factors that limit the capability of ground-based as well as space-based telescopes is the noise components in the signal, which originate from various sources. Broadly, these noise components can be categorized into two types, noise components which are uncorrelated in time, and noise components which are correlated in time. The noise uncorrelated in time originates from several instrumental factors, outliers due to various astronomical phenomena, and in the case of ground-based observations, the variability of Earth's atmosphere. On the other hand, the noise correlated in time originates from stellar activity and pulsations, small-scale variability of the planet-hosting stars, and instrumental effects. Previously, Chakrabarty & Sengupta (2019), Saha et al. (2021), and Saha & Sengupta (2021) developed a critical noise-treatment algorithm using the wavelet-denoising and the Gaussian-process (GP) regression techniques to reduce the noise components, both uncorrelated and correlated in time, from the transit lightcurves. Saha & Sengupta (2021) applied this algorithm to the transit photometric data from TESS and demonstrated its effectiveness in estimating the physical

Table 1
Targets and Observational Details

Target Name	Host Star V_{mag}	Sector	No. of Full Transits
KELT-2 A b	8.68	43–45	16
KELT-3 b	9.82	21, 48	17
KELT-4 A b	9.98	48	7
KELT-11 b	8.04	9	5
KELT-17 b	9.23	44–46	22
KELT-19 A b	9.86	7, 33	4
KELT-20 b	7.59	14, 40, 41, 54	27
KELT-24 b	8.34	14, 20, 21, 40, 41, 47, 48	32
HAT-P-1 b	9.83	56	5
HAT-P-2 b	8.72	24, 25, 51, 52	16
HAT-P-11 b	9.46	14, 15, 41, 54–56	31
HAT-P-22 b	9.76	21, 48	14
HAT-P-69 b	9.77	7, 34	4
HAT-P-70 b	9.47	5, 32	9
MASCARA-4 b	8.19	10, 11, 36, 38	17
XO-3 b	9.85	19	6
WASP-7 b	9.5	27	4
WASP-8 b	9.79	2, 29	4
WASP-14 b	9.75	50	6
WASP-18 b	9.28	2, 3, 29, 30	91
WASP-33 b	8.14	18	16
WASP-69 b	9.87	55, 81	4
WASP-76 b	9.52	30, 42, 43	33
WASP-99 b	9.48	3, 29, 30	12
WASP-136 b	9.97	29, 42	7
WASP-166 b	9.35	8, 35	6
WASP-178 b	9.95	11, 38	7
WASP-189 b	6.6	51	3

properties of the transiting exoplanets more precisely. I have used the same algorithm as was used in Saha & Sengupta (2021) to effectively deal with the noise components present in the TESS transit lightcurves analyzed in this work.

In Section 2, I discuss the target selection and observations; in Section 3, I detail the data analysis and modeling techniques; and finally in Section 4, I discuss the results obtained from this work.

2. Target Selection and Observational Data

For this study, I have selected those transiting exoplanets that orbit around stars with $V_{mag} \leqslant 10$ and have TESS follow-up observational data from one or more than one sectors. The 28 exoplanets selected through this criteria are KELT-2 b, KELT-3 b, KELT-4 A b, KELT-11 b, KELT-17 b, KELT-19 A b, KELT-20 b, KELT-24 b, HAT-P-1 b, HAT-P-2 b, HAT-P-11 b, HAT-P-22 b, HAT-P-69 b, HAT-P-70 b, MASCARA-4 b, XO-3 b, WASP-7 b, WASP-8 b, WASP-14 b, WASP-18 b, WASP-33 b, WASP-69 b, WASP-76 b, WASP-99 b, WASP-136 b, WASP-166 b, WASP-178 b, and WASP-189 b. While most of these exoplanets are hot-to-warm Jupiters, HAT-P-11 b is a warm Neptune, and WASP-166 is a warm Saturn.

The TESS PDCSAP observational lightcurves (Smith et al. 2012; Stumpe et al. 2012, 2014; Jenkins 2017) of these targets was obtained from the public Mikulski Archive for Space Telescopes (MAST).[3] In Table 1, I list the V_{mag} of the host stars (obtained from NASA Exoplanet Archive[4]), the TESS sectors of observations, and the number of full transits observed for each of the target exoplanets.

3. Data Analysis and Modeling

The TESS lightcurves obtained from MAST for each of the targets from each sector spans over ∼27 days. I have identified the full-transit observations in those lightcurves, and sliced them into smaller transit lightcurves, which were used for analysis. Only the full-transit observations were considered in this study, as this removes the possibility of bias due to an incomplete baseline. Also, the TESS observations for the exoplanets targeted in this study had a sufficient number of full-transit observations so as to avoid any bias in the analysis due to insufficient data sets.

The transit lightcurves were then baseline corrected by modeling the out-of-transit sections with a first-order polynomial and subtracting it from the entire lightcurves. Baseline correction removes any large-scale correlated noise components in the signal that are either due to instrumental effects or long-term stellar variability. I refrained from using a higher-order polynomial for baseline correction, as it may induce unwanted distortions in the transit signal in the lightcurves, and also because the GP regression technique would be used at a later stage to remove any shorter-scale correlated noise components.

The lightcurves were then processed with the wavelet-denoising technique (Donoho & Johnstone 1994; Pan et al. 1999; Luo & Zhang 2012; Chakrabarty & Sengupta 2019; Saha & Sengupta 2021; Saha et al. 2021) to reduce the time-uncorrelated fluctuations in the lightcurves. Unlike other smoothing techniques, like binning, the wavelet-denoising technique uses wavelet transform to segregate the low-amplitude noise components from the high-amplitude signal, while preserving the valuable high-frequency components arising from the transit event in the lightcurves. I have followed the same procedure for wavelet denoising as is given by Saha & Sengupta (2021). The analysis uses PyWavelets (Lee et al. 2019) python package for wavelet operations using the Symlet family of wavelets (Daubechies 1988), which are the least asymmetric modified versions of the Daubechies wavelets (Daubechies 1992; Rowe & Abbott 1995). A single level of wavelet transform was used to avoid oversmoothing of the lightcurves, and the widely adopted universal thresholding law (Donoho & Johnstone 1994) was used to estimate the threshold values for the noise level.

To reduce the correlated noise components in the transit lightcurves, I have used the GP regression technique (Rasmussen & Williams 2006; Johnson et al. 2015; Chakrabarty & Sengupta 2019; Pereira et al. 2019; Barros et al. 2020; Saha & Sengupta 2021; Saha et al. 2021). I used the same procedure for GP regression as is discussed in Saha & Sengupta (2021). GP regression is used to model the noise components correlated in time in the lightcurves while simultaneously modeling for the transit signal. While applying GP regression, I used the Matérn class covariance function with the parameter of covariance, $\nu = 3/2$, and two free parameters, i.e., the signal standard deviation α and the characteristic length scale τ, which are used as GP regression model parameters.

[3] https://mast.stsci.edu/portal/Mashup/Clients/Mast/Portal.html

[4] https://exoplanetarchive.ipac.caltech.edu/

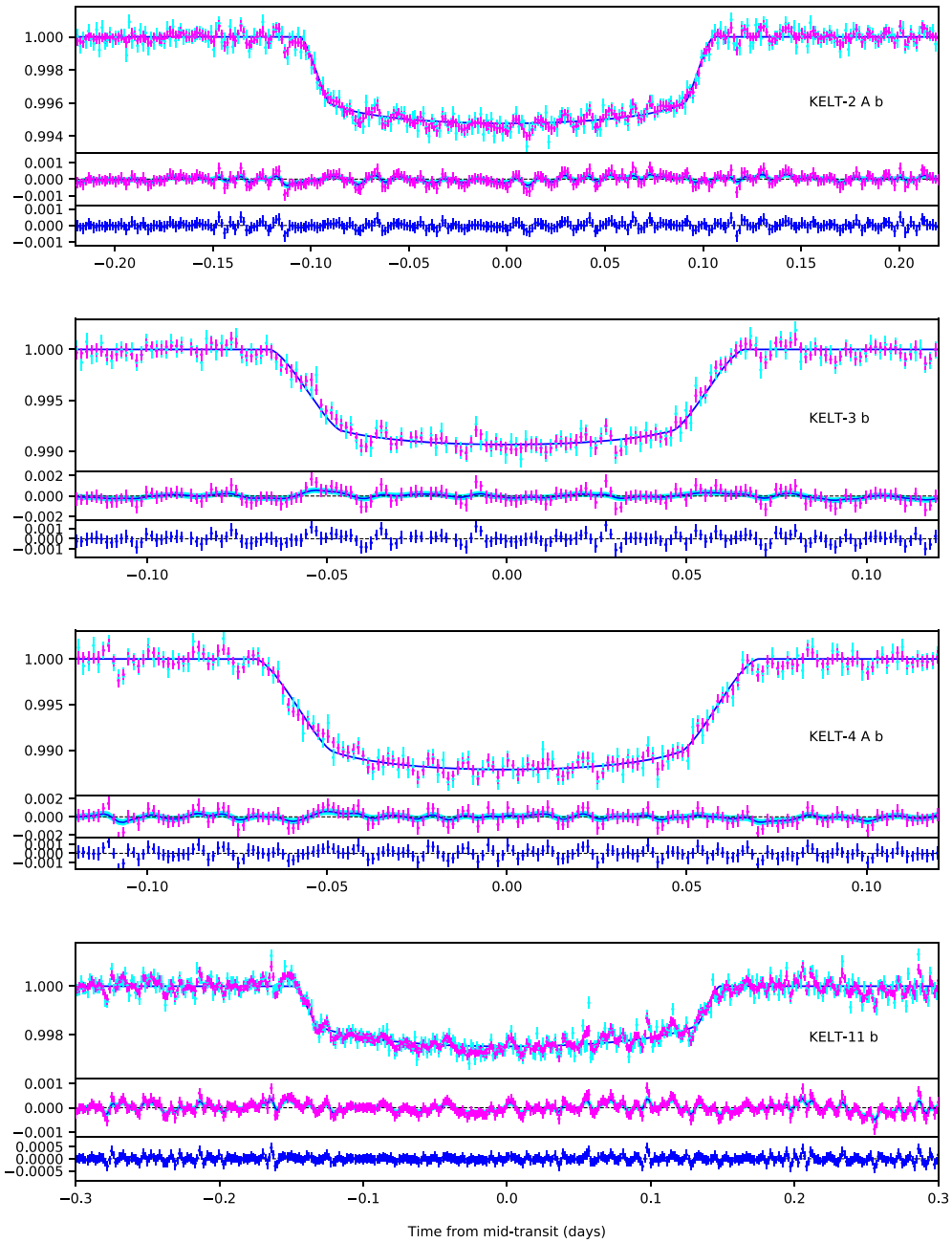

Figure 1. Observed and best-fit model lightcurves (one transit event) for KELT-2 A b, KELT-3 b, KELT-4 A b, and KELT-11 b. For each observed transit, the three sections in each panel show (top) the unprocessed lightcurve (cyan), the lightcurve after wavelet denoising (magenta), and the best-fit transit model (blue); (middle) the residual after modeling without GP regression (magenta), and the mean (blue) and 1σ interval (cyan) of the best-fit GP regression model; (bottom) mean residual flux (blue).

For modeling the transit signature in the lightcurves, the analytical transit formalism by Mandel & Agol (2002) was used, which also incorporates the limb-darkening effect using the quadratic limb-darkening law. The Markov Chain Monte Carlo (MCMC) sampling technique was used to simultaneously model the transit lightcurves for transit signatures and the correlated noise, which incorporated the Metropolis–Hastings algorithm (Hastings 1970).

The directly estimated parameters from modeling the transit lightcurves, b, $R_\star/a$, and $R_p/R_\star$, were used along with the radial velocity and stellar parameters from the previous studies to derive other physical properties for the target exoplanets. The previous studies from which the radial velocity and stellar parameters were adopted are Stassun et al. (2017, 2019), Beatty et al. (2012), Pepper et al. (2013, 2017), Eastman et al. (2016), Zhou et al. (2016). Siverd et al. (2018), Talens et al. (2018), Lund et al. (2017), Hjorth et al. (2019), Rodriguez et al. (2019), Nikolov et al. (2014), Ment et al. (2018), Tsantaki et al. (2014), Yee et al. (2018), Mancini et al. (2018), Bonomo et al. (2017), Zhou et al. (2019), Dorval et al. (2020), Southworth (2012), Knutson et al. (2014), Cortés-Zuleta et al. (2020), Lehmann et al. (2015), West et al. (2016), Hellier et al. (2014, 2019a, 2019b), Lam et al. (2017), Rodríguez Martínez et al. (2020), and Lendl et al. (2020). The

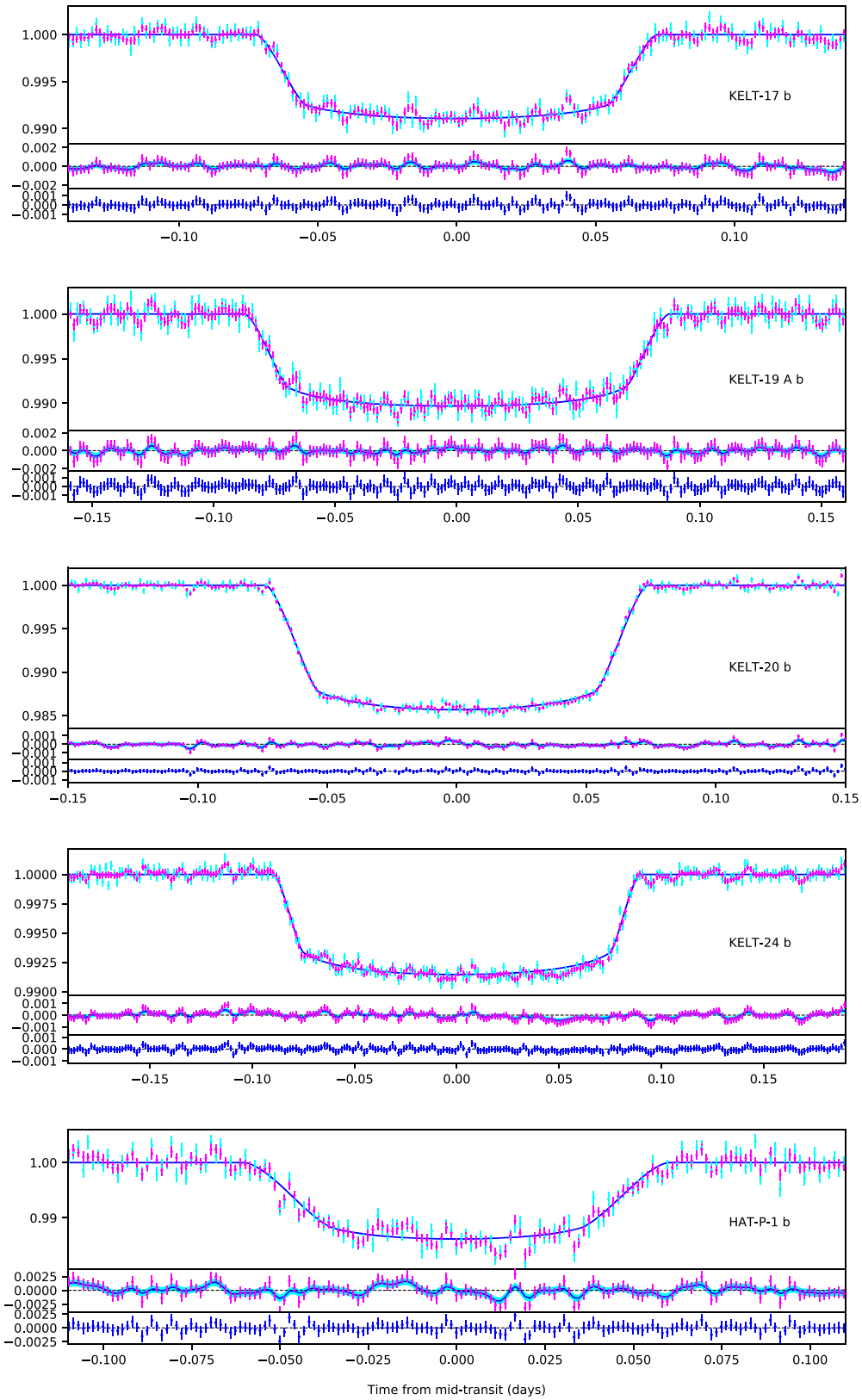

Figure 2. Same as Figure 1, but for KELT-17 b, KELT-19 A b, KELT-20 b, KELT-24 b, and HAT-P-1 b.

midtransit times estimated from modeling the transit lightcurves were used to estimate the transit ephemeris parameters, T_0 and P.

4. Results and Discussions

The transit lightcurves corresponding to one transit event for each of the target exoplanets studied in this work are shown in

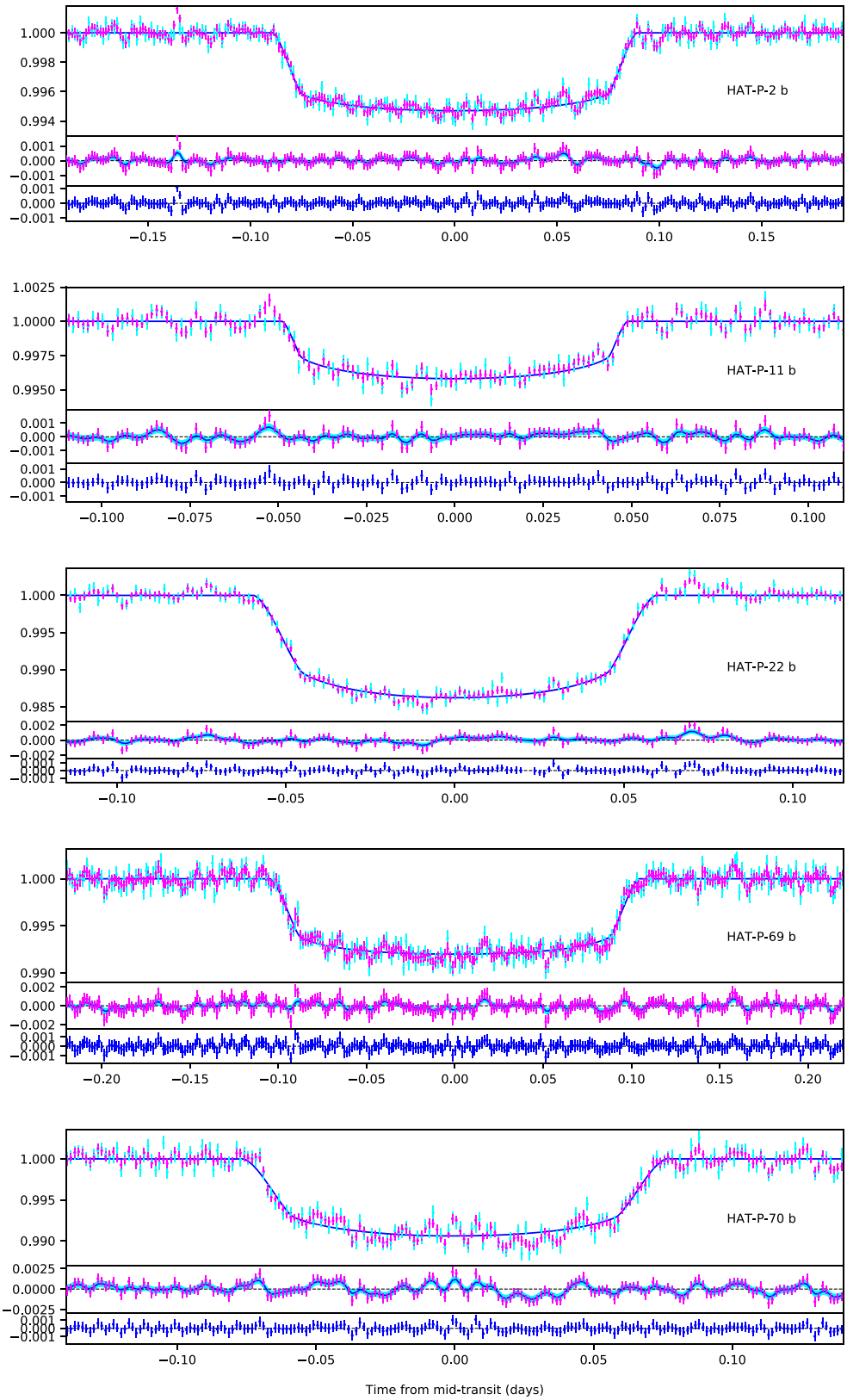

Figure 3. Same as Figure 1, but for HAT-P-2 b, HAT-P-11 b, HAT-P-22 b, HAT-P-69 b, and HAT-P-70 b.

Figures 1–6. The figures show the unprocessed transit lightcurves from TESS data, the lightcurves after wavelet denoising, the best-fit transit model, the residuals without GP regression along with the best-fit GP regression model, and the final residual flux. It can be noticed from these figures that the wavelet-denoising technique has reduced the time-uncorrelated fluctuations in the

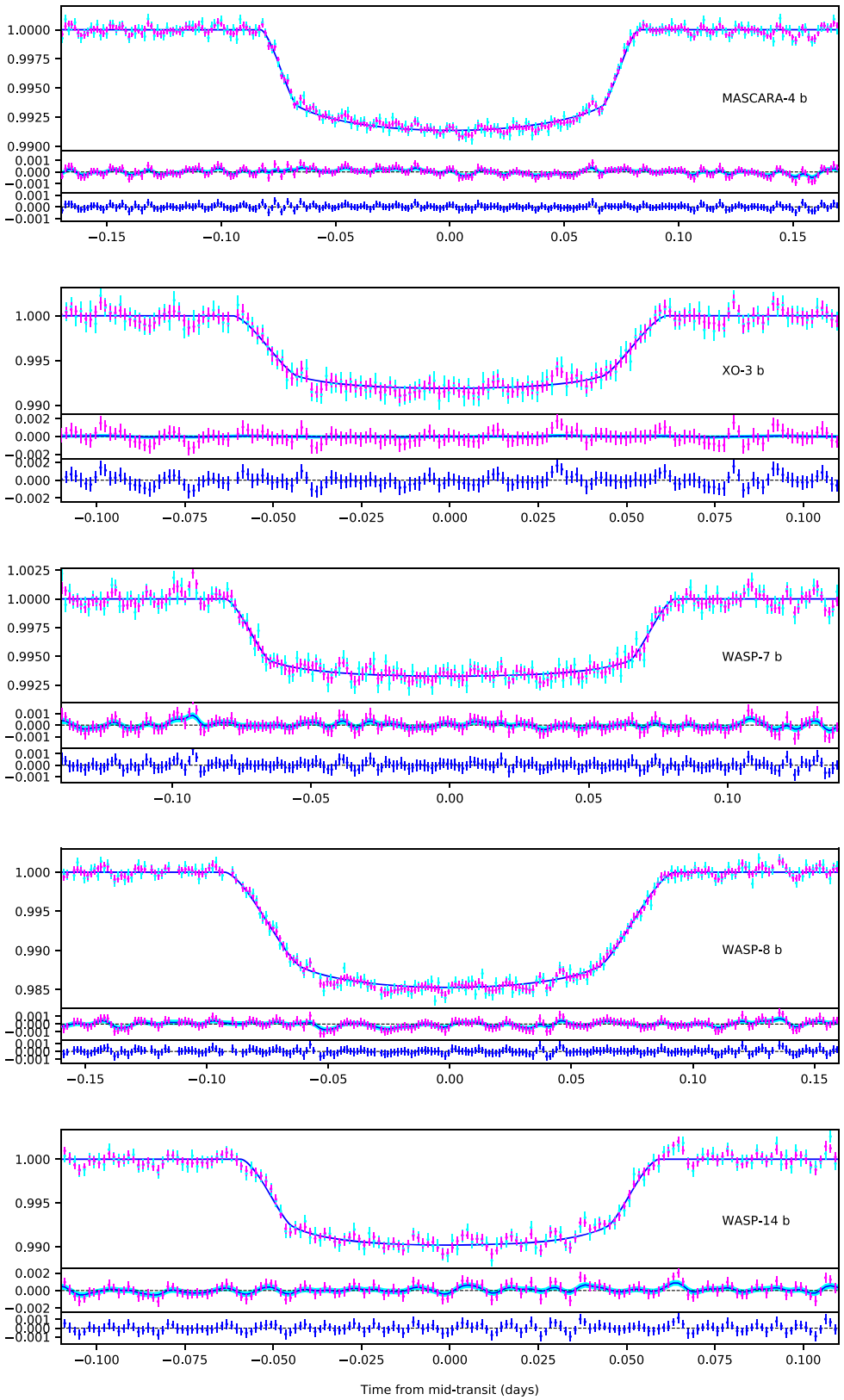

Figure 4. Same as Figure 1, but for MASCARA-4 b, XO-3 b, WASP-7 b, WASP-8 b, and WASP-14 b.

lightcurves without oversmoothing them. This is the advantage of the wavelet-denoising technique over the traditional techniques, like binning, which also crop out the essential higher-frequency signal components from the lightcurves. It can also be seen from the figures that the GP regression technique has modeled the time-correlated noise components quite efficiently to render the

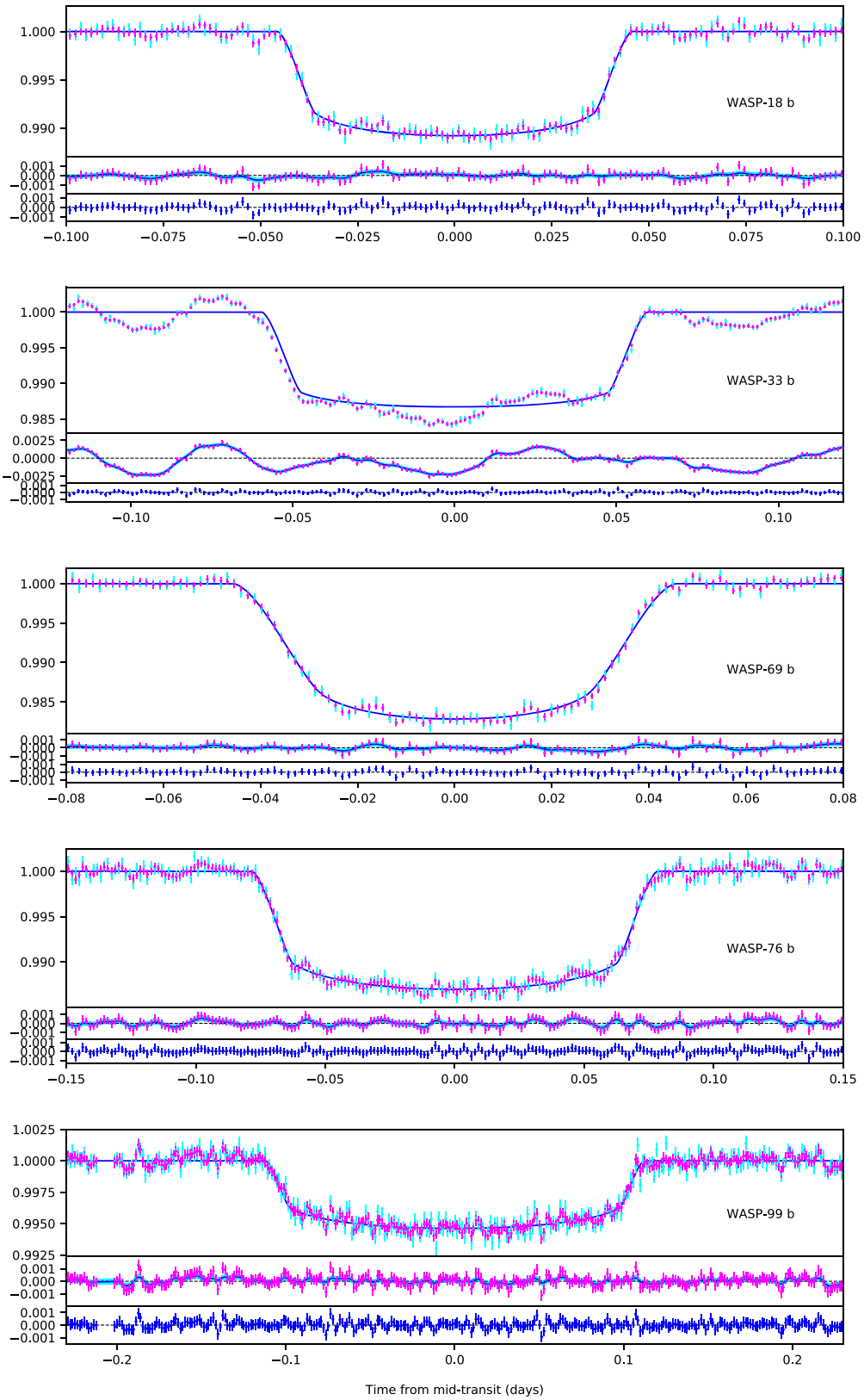

Figure 5. Same as Figure 1, but for WASP-18 b, WASP-33 b, WASP-69 b, WASP-76 b, and WASP-99 b.

final residual flux minimal. One of the major advantages of the GP regression technique is that it can model the correlated noise components with better efficiency for an increase in the S/N of the photometric observations. This is reflected from these figures as well, where the lightcurves with better S/N have the least deviation in the final residual flux.

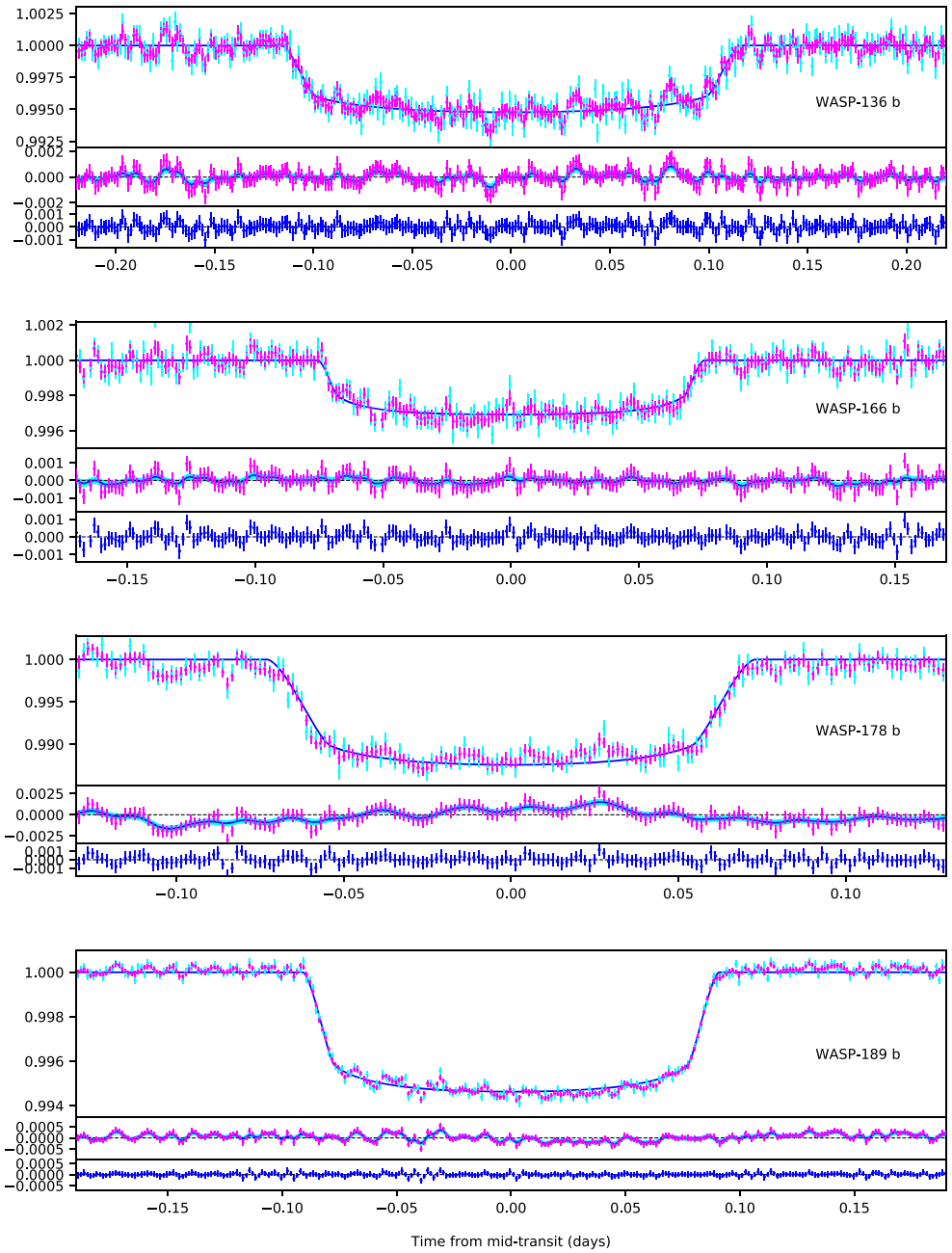

Figure 6. Same as Figure 1, but for WASP-136 b, WASP-166 b, WASP-178 b, and WASP-189 b.

All the physical properties of the target exoplanets estimated in this study are tabulated in Tables 2–8. The best-fit GP regression model parameters are given in Table 9. It can be seen from these tables that the precision in the estimated values of the physical properties from this study are reasonably high, owing to the high-S/N photometric observations from TESS as well as the implementation of the critical noise-treatment algorithm. The corner plots depicting the posterior distribution of the directly estimated transit parameters from the MCMC sampling for KELT-3 b, KELT-20 b, and WASP-18 b are shown in Figures 7–9. These plots show the accuracy in the estimation of the physical properties from this work, and that the uncertainties in the estimated parameters are not underestimated. To understand the extent of improvements in the physical properties for the target exoplanets from this study, the estimated physical properties have been compared with those from the previous studies involving observations from both ground-based as well as space-based instruments.

Comparing the estimated parameters with the previous studies involving only ground-based observations, an improvement in precision in the present study is observed for all the cases. This could be a result of two primary factors. First, the ground-based observations are heavily affected by the noise arising from Earth's atmosphere. Hence, even if ground-based telescopes as large as the 2 m class have been used in some of the studies, the cumulative noise in those observations might be greater than the smaller space-based TESS observations. The second factor is the lack of implementation of any significant

Table 2
Estimated Physical Parameters for KELT-2 A b, KELT-3 b, KELT-4 A b, and KELT-11 b

Parameter	KELT-2 A b	KELT-3 b	KELT-4 A b	KELT-11 b
Transit parameters				
T_0 [BJD_{TDB}]	$2{,}459{,}475.42641^{+0.00017}_{-0.00016}$	$2{,}458{,}872.85409^{+0.00012}_{-0.00013}$	$2{,}459{,}610.39041 \pm 0.00022$	$2{,}458{,}549.07762^{+0.00069}_{-0.00067}$
P [days]	$4.113786^{+0.000016}_{-0.000015}$	$2.70339033 \pm 0.00000065$	2.989582 ± 0.000044	4.73617 ± 0.00027
b	$0.299^{+0.043}_{-0.053}$	$0.671^{+0.01}_{-0.011}$	$0.63^{+0.017}_{-0.016}$	$0.437^{+0.071}_{-0.093}$
$R_\star/a$	$0.1562^{+0.0022}_{-0.0023}$	0.1756 ± 0.002	$0.1602^{+0.0024}_{-0.0022}$	$0.2047^{+0.0083}_{-0.0082}$
$R_p/R_\star$	0.06833 ± 0.00023	$0.09495^{+0.00038}_{-0.00042}$	$0.10698^{+0.00062}_{-0.00082}$	0.04644 ± 0.00051
Limb-darkening coefficients				
C_1	$0.323^{+0.028}_{-0.051}$	$0.308^{+0.058}_{-0.099}$	$0.275^{++0.094}_{-0.164}$	$0.471^{+0.053}_{-0.057}$
C_2	$0.079^{+0.091}_{-0.047}$	$0.111^{+0.13}_{-0.078}$	$0.2^{+0.25}_{-0.13}$	$0.091^{+0.085}_{-0.068}$
Derived parameters				
T_{14} [hr]	5.061 ± 0.012	3.171 ± 0.011	3.259 ± 0.016	$7.112^{+0.04}_{-0.038}$
$a/R_\star$	$6.403^{+0.097}_{-0.09}$	$5.696^{+0.066}_{-0.064}$	$6.242^{+0.089}_{-0.094}$	$4.89^{+0.2}_{-0.19}$
i [deg]	$87.33^{+0.51}_{-0.43}$	$83.23^{+0.19}_{-0.18}$	$84.2^{+0.22}_{-0.25}$	$84.9^{+1.3}_{-1.1}$
M_p [M_J]	$1.52^{+0.077}_{-0.075}$	1.479 ± 0.063	$0.899^{+0.059}_{-0.058}$	0.195 ± 0.018
M_p [$M_\oplus$]	483 ± 24	470 ± 20	286^{+19}_{-18}	62.1 ± 5.9
T_{eq} [K]	1719^{+19}_{-18}	1868 ± 18	1756 ± 25	1717^{+39}_{-37}
a [au]	0.0542 ± 0.0022	0.039 ± 0.0018	0.0465 ± 0.0013	$0.06175^{+0.0046}_{-0.0045}$
R_p [R_J]	$1.12^{+0.046}_{-0.047}$	1.36 ± 0.06	1.668 ± 0.041	1.229 ± 0.078
R_p [$R_\oplus$]	13.57 ± 0.52	15.24 ± 0.67	18.69 ± 0.46	13.78 ± 0.87

Table 3
Estimated Physical Parameters for KELT-17 b, KELT-19 A b, KELT-20 b, and KELT-24 b

Parameter	KELT-17 b	KELT-19 A b	KELT-20 b	KELT-24 b
Transit parameters				
T_0 [BJD_{TDB}]	$2{,}459{,}502.3949 \pm 0.00013$	$2{,}458{,}494.13537^{+0.00034}_{-0.00033}$	$2{,}458{,}684.314347^{+0.000077}_{-0.000078}$	$2{,}458{,}684.816347 \pm 0.000063$
P [days]	$3.0801805^{+0.0000094}_{-0.0000093}$	4.61188 ± 0.00013	$3.47410034 \pm 0.00000034$	$5.55149347 \pm 0.00000055$
b	0.586 ± 0.01	$0.382^{+0.066}_{-0.085}$	$0.5193^{+0.006}_{-0.0058}$	$0.096^{+0.053}_{-0.059}$
$R_\star/a$	$0.1587^{+0.0013}_{-0.0012}$	$0.1156^{+0.0035}_{-0.0034}$	$0.13428^{+0.00051}_{-0.00048}$	$0.09355^{+0.00058}_{-0.00034}$
$R_p/R_\star$	$0.09174^{+0.00028}_{-0.00031}$	$0.09645^{+0.00092}_{-0.00083}$	$0.1157^{+0.00016}_{-0.00017}$	$0.087^{+0.00013}_{-0.00011}$
Limb-darkening coefficients				
C_1	$0.287^{+0.047}_{-0.079}$	$0.196^{+0.089}_{-0.109}$	$0.271^{+0.031}_{-0.029}$	$0.263^{+0.018}_{-0.015}$
C_2	$0.1^{+0.114}_{-0.066}$	$0.28^{+0.21}_{-0.16}$	$0.094^{+0.046}_{-0.048}$	$0.165^{+0.029}_{-0.033}$
Derived parameters				
T_{14} [hr]	$3.4676^{+0.0077}_{-0.0076}$	4.197 ± 0.027	3.538 ± 0.004	$4.3038^{+0.0045}_{-0.0042}$
$a/R_\star$	$6.302^{+0.049}_{-0.051}$	8.65 ± 0.26	$7.447^{+0.027}_{-0.028}$	$10.689^{+0.039}_{-0.066}$
i [deg]	84.66 ± 0.13	$87.47^{+0.62}_{-0.53}$	$86.001^{+0.058}_{-0.061}$	$89.49^{+0.31}_{-0.29}$
M_p [M_J]	1.3 ± 0.28	$3.98^{+0.32}_{-0.33}$	$3.355^{+0.062}_{-0.063}$	4.65 ± 0.16
M_p [$M_\oplus$]	415^{+90}_{-89}	1265^{+101}_{-106}	1129 ± 20	1478^{+51}_{-50}
T_{eq} [K]	2100 ± 16	1802^{+37}_{-36}	2329 ± 24	1408 ± 11
a [au]	$0.0482^{+0.0017}_{-0.0016}$	0.0736 ± 0.0044	0.056 ± 0.0014	$0.0748^{+0.0011}_{-0.0012}$
R_p [R_J]	1.469 ± 0.049	$1.717^{+0.094}_{-0.093}$	1.821 ± 0.045	1.275 ± 0.019
R_p [$R_\oplus$]	16.46 ± 0.55	19.2 ± 1	$20.41^{+0.51}_{-0.5}$	14.29 ± 0.21

noise reduction technique in the previous studies, which has left the reducible noise components (such as correlated noise) untreated, and has contributed toward the larger uncertainties in the estimated parameters.

On the other hand, comparing the estimated properties with the previous studies involving space-based observations would be more interesting. Since all the target exoplanets studied in this work are around bright host stars, several of them have previously been studied using observations from TESS as well as other space-based instruments. A comparison between them would give both qualitative and quantitative ideas about the capability of different instruments and differences in the results from different approaches. I have compared the three primary transit parameters, b, $R_p/R_\star$, and $a/R_\star$ from the present work and those from the previous studies, as listed in Table 10. b and $R_p/R_\star$ were estimated directly from modeling the transit lightcurves, whereas $a/R_\star$ was derived from the directly estimated $R_\star/a$ in the present study.

When comparing the studies involving larger space-based telescopes than TESS, such as Spitzer, Hubble Space Telescope (HST), Kepler, and CHaracterising ExOPlanet Satellite (CHEOPS), a less precise estimation in the transit parameters is expected than in the previous studies. However, this has not always been reflected from the comparison and is detailed as follows. Beatty et al. (2017) have studied KELT-11 b using Spitzer observations, and their estimated values of b and $a/R_\star$ are more precise than the present study, but that of $R_p/R_\star$ is less precise than the present study. Garai et al. (2022) studied

Table 4
Estimated Physical Parameters for HAT-P-1 b, HAT-P-2 b, HAT-P-11 b, and HAT-P-22 b

Parameter	HAT-P-1 b	HAT-P-2 b	HAT-P-11 b	HAT-P-22 b
Transit parameters				
T_0 [BJD$_{\rm TDB}$]	$2{,}459{,}829.47609^{+0.0005}_{-0.00049}$	$2{,}458{,}956.23792 \pm 0.00013$	$2{,}458{,}687.20645^{+0.00015}_{-0.00014}$	$2{,}458{,}871.629976 \pm 0.000089$
P [days]	$4.46508^{+0.00016}_{-0.00015}$	5.6334665 ± 0.0000014	$4.88780248 \pm 0.00000081$	$3.21223293 \pm 0.00000058$
b	$0.733^{+0.021}_{-0.029}$	$0.456^{+0.027}_{-0.034}$	$0.107^{+0.071}_{-0.081}$	$0.441^{+0.022}_{-0.028}$
$R_\star/a$	$0.1^{+0.0028}_{-0.0027}$	$0.1025^{+0.0015}_{-0.0017}$	$0.05968^{+0.00055}_{-0.00035}$	$0.114^{+0.0012}_{-0.0014}$
$R_p/R_\star$	$0.1161^{+0.0013}_{-0.0015}$	$0.06967^{+0.00026}_{-0.00031}$	$0.05885^{+0.00024}_{-0.0003}$	$0.11019^{+0.0005}_{-0.00066}$
Limb-darkening coefficients				
C_1	0.22 ± 0.15	$0.301^{+0.046}_{-0.05}$	$0.488^{+0.037}_{-0.06}$	$0.403^{+0.056}_{-0.065}$
C_2	$0.36^{+0.22}_{-0.21}$	$0.099^{+0.077}_{-0.075}$	$0.094^{+0.112}_{-0.059}$	$0.147^{+0.116}_{-0.099}$
Derived parameters				
T_{14} [hr]	$2.886^{+0.04}_{-0.037}$	$4.2778^{+0.0102}_{-0.0099}$	$2.3479^{+0.0067}_{-0.0061}$	$2.8598^{+0.0087}_{-0.009}$
$a/R_\star$	$10^{+0.28}_{-0.27}$	$9.76^{+0.17}_{-0.14}$	$16.756^{+0.098}_{-0.154}$	$8.774^{+0.113}_{-0.094}$
i [deg]	$85.8^{+0.28}_{-0.24}$	$87.32^{+0.24}_{-0.2}$	$89.63^{+0.28}_{-0.25}$	$87.12^{+0.22}_{-0.18}$
M_p [$M_{\rm J}$]	0.525 ± 0.019	$10.1^{+0.15}_{-0.16}$	0.224 ± 0.01	$2.17^{+0.055}_{-0.056}$
M_p [$M_\oplus$]	$166.9^{+6}_{-5.9}$	3211^{+49}_{-50}	71.2 ± 3.2	690^{+17}_{-18}
$T_{\rm eq}$ [K]	1337^{+21}_{-22}	1452 ± 16	$826.3^{+9.2}_{-9.1}$	1268 ± 14
a [au]	$0.0546^{+0.002}_{-0.0019}$	$0.0777^{+0.003}_{-0.0029}$	$0.05316^{+0.00079}_{-0.00081}$	$0.0425^{+0.0019}_{-0.0018}$
R_p [$R_{\rm J}$]	$1.326^{+0.034}_{-0.035}$	1.159 ± 0.041	0.391 ± 0.0054	1.115 ± 0.047
R_p [$R_\oplus$]	$14.86^{+0.38}_{-0.39}$	12.99 ± 0.46	4.383 ± 0.061	$12.5^{+0.52}_{-0.53}$

Table 5
Estimated Physical Parameters for HAT-P-69 b, HAT-P-70 b, MASCARA-4 b, and XO-3 b

Parameter	HAT-P-69 b	HAT-P-70 b	MASCARA-4 b	XO-3 b
Transit parameters				
T_0 [BJD$_{\rm TDB}$]	$2{,}459{,}232.985 \pm 0.0005$	$2{,}459{,}175.05307^{+0.00037}_{-0.00036}$	$2{,}459{,}282.43841 \pm 0.0001$	$2{,}458{,}819.06409 \pm 0.00026$
P [days]	4.78689 ± 0.00018	2.744219 ± 0.000065	$2.8240776^{+0.0000061}_{-0.0000059}$	$3.191585^{+0.000071}_{-0.000072}$
b	$0.23^{+0.12}_{-0.16}$	$0.554^{+0.03}_{-0.043}$	$0.396^{+0.018}_{-0.019}$	$0.694^{+0.027}_{-0.029}$
$R_\star/a$	$0.1292^{+0.0047}_{-0.0028}$	$0.1837^{+0.004}_{-0.0051}$	$0.1802^{+0.14}_{-0.15}$	0.143 ± 0.0044
$R_p/R_\star$	$0.08453^{+0.00073}_{-0.0007}$	$0.0924^{+0.00075}_{-0.00088}$	$0.08737^{+0.0002}_{-0.00022}$	$0.08826^{+0.00075}_{-0.00069}$
Limb-darkening coefficients				
C_1	$0.251^{+0.08}_{-0.093}$	$0.409^{+0.07}_{-0.105}$	$0.428^{+0.017}_{-0.024}$	$0.14^{+0.104}_{-0.093}$
C_2	$0.19^{+0.18}_{-0.13}$	$0.14^{+0.15}_{-0.1}$	$0.035^{+0.036}_{-0.024}$	0.37 ± 0.14
Derived parameters				
T_{14} [hr]	$5.027^{+0.031}_{-0.028}$	$3.661^{+0.15}_{-0.12}$	$3.97^{+0.0072}_{-0.0074}$	$2.944^{+0.021}_{-0.022}$
$a/R_\star$	$7.74^{+0.17}_{-0.27}$	$5.44^{+0.15}_{-0.12}$	$5.549^{+0.045}_{-0.044}$	$6.99^{+0.22}_{-0.21}$
i [deg]	$88.29^{+1.19}_{-0.99}$	$84.15^{+0.6}_{-0.44}$	85.91 ± 0.22	84.31 ± 0.4
M_p [$M_{\rm J}$]	3.58 ± 0.57	6.87 ± 0.025	$3.15^{+0.9}_{-0.91}$	12.16 ± 0.44
M_p [$M_\oplus$]	1137^{+180}_{-182}	$2183.4^{+7.8}_{-7.9}$	1000^{+287}_{-288}	3865^{+139}_{-141}
$T_{\rm eq}$ [K]	1953^{+45}_{-41}	2643^{+43}_{-45}	2455^{+41}_{-40}	1719^{+29}_{-30}
a [au]	$0.0692^{+0.002}_{-0.0025}$	0.0499 ± 0.002	0.0474 ± 0.0015	$0.0448^{+0.003}_{-0.0029}$
R_p [$R_{\rm J}$]	1.584 ± 0.029	$1.771^{+0.06}_{-0.059}$	1.561 ± 0.048	$1.183^{+0.072}_{-0.071}$
R_p [$R_\oplus$]	17.76 ± 0.32	19.85 ± 0.67	$17.5^{+0.54}_{-0.53}$	13.26 ± 0.8

KELT-17 b and KELT-19 A b using CHEOPS and TESS observations. For KELT-17 b, the estimated values of all three parameters, b, $R_p/R_\star$, and $a/R_\star$, from their study are less precise than the present study. However, for KELT-19 b, their estimated values of b and $a/R_\star$ are more precise than the present study, but that of $R_p/R_\star$ is less precise than the present study. Nikolov et al. (2014) have studied HAT-P-1 b using HST observations and their estimated values of all three parameters, b, $R_p/R_\star$, and $a/R_\star$, are more precise than the present study. Sanchis-Ojeda & Winn (2011) studied HAT-P-11 b using Kepler observations, and their estimated value of b is more precise than the present study, but those of $R_p/R_\star$ and $a/R_\star$ are less precise than the present study. Lendl et al. (2020) studied WASP-189 b using CHEOPS observations, and their estimated values of all three parameters, b, $R_p/R_\star$, and $a/R_\star$, are more precise than the present study.

Now, moving toward the previous studies involving observations from TESS, Patel & Espinoza (2022) studied a number of transiting systems, of which KELT-11 b, KELT-20 b, KELT-24 b, HAT-P-2 b, HAT-P-69 b, HAT-P-70 b, XO-3 b, WASP-7 b, WASP-99 b, WASP-136 b, and WASP-166 b are also in the present study. By comparing the estimated parameters, except for a few cases such as b and $a/R_\star$ for KELT-11 b, b for HAT-P-69 b, b and $a/R_\star$ for HAT-P-70 b, and b and $a/R_\star$ for WASP-7 b, the precision is better in the present study compared to Patel & Espinoza (2022). Hord et al. (2021) also studied a number of transiting exoplanets, of which KELT-11 b, KELT-19 A b, HAT-P-69 b, HAT-P-70 b, WASP-

Table 6
Estimated Physical Parameters for WASP-7 b, WASP-8 b, WASP-14 b, and WASP-18 b

Parameter	WASP-7 b	WASP-8 b	WASP-14 b	WASP-18 b
Transit parameters				
T_0 [BJD$_{\rm TDB}$]	$2{,}459{,}038.75846^{+0.00037}_{-0.00038}$	$2{,}458{,}358.92063^{+0.00026}_{-0.00027}$	$2{,}459{,}671.35858 \pm 0.00022$	$2{,}458{,}354.457864^{+0.000047}_{-0.000048}$
P [days]	$4.95468^{+0.00015}_{-0.00014}$	8.1587277 ± 0.000004	$2.243832^{+0.000045}_{-0.000046}$	$0.941452531 \pm 0.000000085$
b	$0.532^{+0.046}_{-0.049}$	0.64 ± 0.018	$0.545^{+0.033}_{-0.052}$	$0.395^{+0.019}_{-0.022}$
$R_\star/a$	$0.109^{+0.0037}_{-0.0033}$	$0.0777^{+0.0013}_{-0.0012}$	$0.1731^{+0.004}_{-0.0051}$	$0.2907^{+0.0021}_{-0.0023}$
$R_p/R_\star$	$0.07892^{+0.00063}_{-0.00065}$	$0.11747^{+0.00087}_{-0.00102}$	$0.09435^{+0.00083}_{-0.00121}$	$0.09836^{+0.0003}_{-0.00032}$
Limb-darkening coefficients				
C_1	0.17 ± 0.11	$0.3^{+0.12}_{-0.17}$	$0.122^{+0.103}_{-0.088}$	$0.282^{+0.045}_{-0.048}$
C_2	$0.29^{+0.18}_{-0.16}$	$0.26^{+0.25}_{-0.18}$	$0.5^{+0.16}_{-0.18}$	$0.189^{+0.081}_{-0.081}$
Derived parameters				
T_{14} [hr]	3.885 ± 0.027	$4.449^{+0.025}_{-0.023}$	2.842 ± 0.017	2.1907 ± 0.0047
$a/R_\star$	$9.17^{+0.29}_{-0.3}$	$12.87^{+0.19}_{-0.21}$	$5.78^{+0.18}_{-0.13}$	$3.44^{+0.028}_{-0.025}$
i [deg]	$86.67^{+0.39}_{-0.41}$	$87.15^{+0.12}_{-0.13}$	$84.58^{+0.67}_{-0.45}$	$83.4^{+0.41}_{-0.36}$
M_p [$M_{\rm J}$]	$1.123^{+0.084}_{-0.083}$	$2.247^{+0.078}_{-0.08}$	$7.3^{+0.48}_{-0.49}$	$10.48^{+0.32}_{-0.33}$
M_p [$M_\oplus$]	356^{+27}_{-26}	714 ± 25	2319^{+151}_{-156}	3332^{+103}_{-106}
$T_{\rm eq}$ [K]	1522^{+30}_{-29}	1104 ± 18	1903^{+39}_{-40}	2452^{+21}_{-20}
a [au]	$0.0626^{+0.0032}_{-0.0031}$	0.0616 ± 0.0026	$0.0357^{+0.0019}_{-0.0018}$	0.021105 ± 0.00098
R_p [$R_{\rm J}$]	1.128 ± 0.045	$1.177^{+0.047}_{-0.046}$	1.216 ± 0.054	1.263 ± 0.058
R_p [$R_\oplus$]	12.64 ± 0.5	$13.19^{+0.52}_{-0.51}$	$13.63^{+0.6}_{-0.61}$	14.15 ± 0.65

Table 7
Estimated Physical Parameters for WASP-33 b, WASP-69 b, WASP-76 b, and WASP-99 b

Parameter	WASP-33 b	WASP-69 b	WASP-76 b	WASP-99 b
Transit parameters				
T_0 [BJD$_{\rm TDB}$]	$2{,}458{,}792.63408 \pm 0.00014$	$2{,}459{,}798.77552 \pm 0.00014$	$2{,}459{,}117.687167^{+0.000073}_{-0.000072}$	$2{,}458{,}387.96013 \pm 0.00027$
P [days]	1.219888 ± 0.000014	3.868143 ± 0.000044	$1.80988122 \pm 0.00000046$	5.7525842 ± 0.0000025
b	$0.06^{0.065}_{-0.04}$	$0.694^{+0.014}_{-0.017}$	$0.172^{+0.04}_{-0.055}$	$0.109^{+0.077}_{-0.069}$
$R_\star/a$	$0.27236^{+0.0013}_{-0.00069}$	$0.08326^{+0.00109}_{-0.00099}$	0.2454 ± 0.0017	$0.11507^{+0.00124}_{-0.00064}$
$R_p/R_\star$	$0.11036^{+0.00071}_{-0.00064}$	$0.1271^{+0.0011}_{-0.0012}$	$0.10704^{+0.00026}_{-0.00027}$	$0.06774^{+0.00024}_{-0.00022}$
Limb-darkening coefficients				
C_1	$0.184^{+0.073}_{-0.088}$	$0.124^{+0.145}_{-0.089}$	$0.32^{+0.021}_{-0.024}$	$0.395^{+0.04}_{-0.046}$
C_2	$0.142^{+0.124}_{-0.096}$	$0.59^{+0.17}_{-0.23}$	$0.116^{+0.05}_{-0.044}$	$0.113^{+0.084}_{-0.071}$
Derived parameters				
T_{14} [hr]	$2.858^{+0.006}_{-0.0056}$	2.193 ± 0.014	$3.7605^{+0.0054}_{-0.0051}$	5.384 ± 0.012
$a/R_\star$	$3.6716^{+0.0093}_{-0.0175}$	12.01 ± 0.15	4.075 ± 0.028	$8.691^{+0.049}_{-0.093}$
i [deg]	$89.07^{+0.63}_{-1.02}$	86.69 ± 0.11	$87.58^{+0.79}_{-0.59}$	$89.28^{+0.45}_{-0.52}$
M_p [$M_{\rm J}$]	$1.41^{+0.14}_{-0.13}$	$0.259^{+0.018}_{-0.017}$	0.921 ± 0.032	$2.77^{+0.12}_{-0.13}$
M_p [$M_\oplus$]	449^{+44}_{-43}	$82.4^{+5.6}_{-5.5}$	293 ± 10	882 ± 40
$T_{\rm eq}$ [K]	1851 ± 34	959 ± 12	2190 ± 35	1484 ± 25
a [au]	0.01364 ± 0.00065	$0.0454^{+0.0017}_{-0.0016}$	0.03277 ± 0.00078	0.0689 ± 0.003
R_p [$R_{\rm J}$]	0.858 ± 0.041	$1.006^{+0.035}_{-0.036}$	1.802 ± 0.042	1.127 ± 0.048
R_p [$R_\oplus$]	9.62 ± 0.46	11.28 ± 0.4	20.2 ± 0.47	12.63 ± 0.54

8 b, and WASP-178 b are also in the present study. By comparing the estimated parameters for this case, however, the precision from the present study is better for all the targets compared to the previous work. Maciejewski (2020) studied KELT-24 b using TESS observations, however their precision in the estimated parameters is worse than in the present study. Zhou et al. (2019) studied HAT-P-69 b and HAT-p-70 b using TESS observations. For HAT-P-69 b, the estimated values of b and $a/R_\star$ from Zhou et al. (2019) are more precise compared to the present study, while that of $R_p/R_\star$ is more precise in the present study. However, for HAT-P-70 b the estimated values of all three parameters, b, $R_p/R_\star$, and $a/R_\star$, are more precise in the present study. Compared to Wong et al. (2014), who studied XO-3 b using observations from Spitzer, the estimated values of $R_p/R_\star$ and $a/R_\star$ are less precise in the present study. Cortés-Zuleta et al. (2020), who studied WASP-18 b, have estimated values for all three parameters, b, $R_p/R_\star$, and $a/R_\star$, that are less precise than the present study. von Essen et al. (2020), who studied WASP-33 b using TESS observations, have estimated parameters that are more precise than the present study. Rodríguez Martínez et al. (2020), who studied WASP-178 b using TESS observations, have estimated values of b and $R_p/R_\star$ that are more precise than the present study, whereas their estimated value of $a/R_\star$ is less precise.

Summarizing the above discussions, the precision of the impact factor, b, has improved for KELT-3 b, KELT-4 A b, KELT-17 b, KELT-20 b, KELT-24 b, HAT-P-2 b, HAT-P-22 b, MASCARA-4 b, WASP-8 b, WASP-14 b, WASP-18 b,

Table 8
Estimated Physical Parameters for WASP-136 b, WASP-166 b, WASP-178 b, and WASP-189 b

Parameter	WASP-136 b	WASP-166 b	WASP-178 b	WASP-189 b
Transit parameters				
T_0 [BJD_{TDB}]	$2{,}459{,}092.52455 \pm 0.00036$	$2{,}458{,}518.96491 \pm 0.00034$	$2{,}459{,}338.69747^{+0.00025}_{-0.00026}$	$2{,}459{,}700.16634^{+0.00019}_{-0.00018}$
P [days]	5.215351 ± 0.0000079	5.4435455 ± 0.0000035	3.34488 ± 0.00013	$2.724099^{+0.000051}_{-0.000052}$
b	$0.331^{+0.078}_{-0.103}$	$0.129^{+0.09}_{-0.085}$	$0.514^{+0.035}_{-0.045}$	$0.358^{+0.047}_{-0.052}$
$R_\star/a$	$0.1369^{+0.0046}_{-0.004}$	$0.083382^{+0.00094}_{-0.001}$	$0.1388^{+0.0029}_{-0.0033}$	$0.2057^{+0.004}_{-0.0036}$
$R_p/R_\star$	$0.0683^{+0.00051}_{-0.00052}$	$0.05158^{+0.0004}_{-0.00041}$	$0.1068^{+0.00092}_{-0.0012}$	0.06984 ± 0.00032
Limb-darkening coefficients				
C_1	$0.307^{+0.055}_{-0.083}$	$0.17^{+0.14}_{-0.1}$	$0.24^{+0.1}_{-0.11}$	$0.18^{+0.081}_{-0.084}$
C_2	$0.131^{+0.138}_{-0.082}$	$0.48^{+0.22}_{-0.22}$	$0.24^{+0.21}_{-0.17}$	0.27 ± 0.13
Derived parameters				
T_{14} [hr]	$5.566^{+0.032}_{-0.029}$	$3.61^{+0.023}_{-0.02}$	3.497 ± 0.023	4.41 ± 0.02
$a/R_\star$	$7.31^{+0.22}_{-0.24}$	$11.99^{+0.15}_{-0.13}$	$7.2^{+0.17}_{-0.15}$	$4.582^{+0.03}_{-0.037}$
i [deg]	$87.4^{+0.86}_{-0.72}$	$89.38^{+0.41}_{-0.44}$	$85.9^{+0.45}_{-0.36}$	$84.02^{+0.21}_{-0.16}$
M_p [M_J]	1.74 ± 0.11	0.0982 ± 0.0051	1.66 ± 0.12	2.01 ± 0.15
M_p [$M_\oplus$]	554^{+35}_{-34}	31.2 ± 1.6	529 ± 39	640^{+48}_{-47}
T_{eq} [K]	1638^{+36}_{-34}	1235 ± 12	2465 ± 47	2643 ± 28
a [au]	0.0811 ± 0.004	0.0699 ± 0.0024	$0.0603^{+0.0021}_{-0.002}$	0.05027 ± 0.00074
R_p [R_J]	1.589 ± 0.064	0.629 ± 0.021	1.87 ± 0.053	1.381 ± 0.045
R_p [$R_\oplus$]	17.81 ± 0.72	7.05 ± 0.24	20.96 ± 0.59	15.48 ± 0.51

Table 9
Best-fit Gaussian-process (GP) Regression Model Parameters

Target	α	τ
KELT-2 A b	$0.000191^{+0.000013}_{-0.000012}$	$0.00168^{+0.00021}_{-0.00023}$
KELT-3 b	0.000278 ± 0.000036	$0.00379^{+0.00152}_{-0.00078}$
KELT-4 A b	$0.000262^{+0.000037}_{-0.000032}$	$0.00272^{+0.00038}_{-0.00034}$
KELT-11 b	$0.0001753^{+0.0000087}_{-0.000008}$	$0.00297^{+0.00022}_{-0.00021}$
KELT-17 b	$0.000294^{+0.000024}_{-0.000023}$	$0.00289^{+0.00029}_{-0.00031}$
KELT-19 A b	$0.000399^{+0.000032}_{-0.000028}$	$0.00254^{+0.0003}_{-0.00024}$
KELT-20 b	$0.000262^{+0.000014}_{-0.000011}$	$0.00275^{+0.00023}_{-0.00019}$
KELT-24 b	$0.000191^{+0.000013}_{-0.000012}$	$0.00268^{+0.00021}_{-0.00023}$
HAT-P-1 b	$0.000849^{+0.000062}_{-0.000058}$	$0.00255^{+0.0003}_{-0.00024}$
HAT-P-2 b	$0.000221^{+0.000013}_{-0.000014}$	$0.00277^{+0.00026}_{-0.00024}$
HAT-P-11 b	$0.000325^{+0.000023}_{-0.000024}$	$0.00253^{+0.00022}_{-0.0002}$
HAT-P-22 b	$0.000248^{+0.000031}_{-0.000028}$	$0.00324^{+0.00044}_{-0.00042}$
HAT-P-69 b	$0.000394^{+0.000023}_{-0.000025}$	$0.003^{+0.00029}_{-0.00028}$
HAT-P-70 b	$0.000591^{+0.000032}_{-0.00003}$	$0.00267^{+0.00023}_{-0.0002}$
MASCARA-4 b	$0.000222^{+0.000012}_{-0.000014}$	0.00289 ± 0.00026
XO-3 b	$0.00011^{+0.00006}_{-0.000063}$	$0.00436^{+0.0031}_{-0.0015}$
WASP-7 b	$0.000305^{+0.000019}_{-0.000022}$	$0.00279^{+0.00027}_{-0.00024}$
WASP-8 b	$0.00035^{+0.000022}_{-0.000023}$	$0.0037^{+0.00039}_{-0.00027}$
WASP-14 b	$0.000352^{+0.000028}_{-0.000027}$	$0.00268^{+0.00037}_{-0.00029}$
WASP-18 b	0.000251 ± 0.000026	$0.00335^{+0.00093}_{-0.00063}$
WASP-33 b	$0.00111^{+0.000098}_{-0.000095}$	$0.0127^{+0.0014}_{-0.0011}$
WASP-69 b	$0.000302^{+0.000032}_{-0.00003}$	$0.00298^{+0.00057}_{-0.00041}$
WASP-76 b	$0.00034^{+0.000019}_{-0.000022}$	$0.00259^{+0.00026}_{-0.00022}$
WASP- 99 b	0.000231 ± 0.000018	$0.00307^{+0.00032}_{-0.00034}$
WASP-136 b	$0.000347^{+0.000029}_{-0.000024}$	$0.00289^{+0.00034}_{-0.00028}$
WASP-166 b	$0.000211^{+0.000021}_{-0.000019}$	0.00295 ± 0.00025
WASP-178 b	$0.000662^{+0.00006}_{-0.000051}$	$0.00874^{+0.0028}_{-0.0017}$
WASP-189 b	$0.0001613^{+0.0000069}_{-0.0000061}$	$0.00315^{+0.00015}_{-0.00017}$

WASP-69 b, WASP-76 b, WASP-99 b, WASP-136 b, and WASP-166 b compared to previous studies. The improvements have been up to an order of magnitude compared to the most precise values known from previous studies. Also, the estimated value of b for KELT-2 A b has not been given by any of the previous studies, and it is estimated and updated in the present study.

For the case of $R_p/R_\star$, the precision has improved for KELT-3 b, KELT-4 A b, KELT-11 b, KELT-17 b, KELT-19 A b, KELT-20 b, KELT-24 b, HAT-P-2 b, HAT-P-11 b, HAT-P-22 b, HAT-P-69 b, HAT-P-70 b, MASCARA-4 b, WASP-7 b, WASP-8 b, WASP-18 b, WASP-99 b, WASP-136 b, and WASP-166 b compared to the best-known values from the previous studies for up to 2 orders of magnitude. For the cases of KELT-2 A b, WASP-69 b, and WASP-76 b, the estimated values of $R_p/R_\star$ were not given by any of the previous studies, and these are estimated and updated in the present study.

For the case of $a/R_\star$, the precision has improved for KELT-2 A b, KELT-3 b, KELT-4 A b, KELT-17 b, KELT-20 b, KELT-24 b, HAT-P-2 b, HAT-P-11 b, HAT-P-22 b, MASCARA-4 b, WASP-8 b, WASP-18 b, WASP-69 b, WASP-99 b, WASP-136 b, WASP-166 b, and WASP-178 b compared to the best-known values from the previous studies for up to 1 order of magnitude. For the case of WASP-76 b, the estimated value of $R_\star/a$ is not given by any of the previous studies, and it is estimated and updated in the present study.

When comparing this study with previous studies, it can be noted that for most of the cases, the estimated physical properties from this study vary slightly to significantly compared to the previous studies. While the precision of an estimated parameter depends upon the S/N of the photometric lightcurves and further noise treatments, the accuracy of the values of estimated parameters can still change depending upon the observational and data reduction bias, unidentified noise sources in the lightcurves, insufficient data sets, and inaccurate approaches in data analysis and modeling. For studies involving ground-based observations, the chances of observational bias while incorporating various atmospheric factors is quite high. The noise due to various atmospheric perturbations, if unattended, can also contribute to inaccurate estimation of the physical properties. Being a space-based instrument, TESS provides observations unaffected by Earth's atmosphere, and hence the data do not contain any correlated or other sources of noise due to the interference of Earth's atmosphere. This

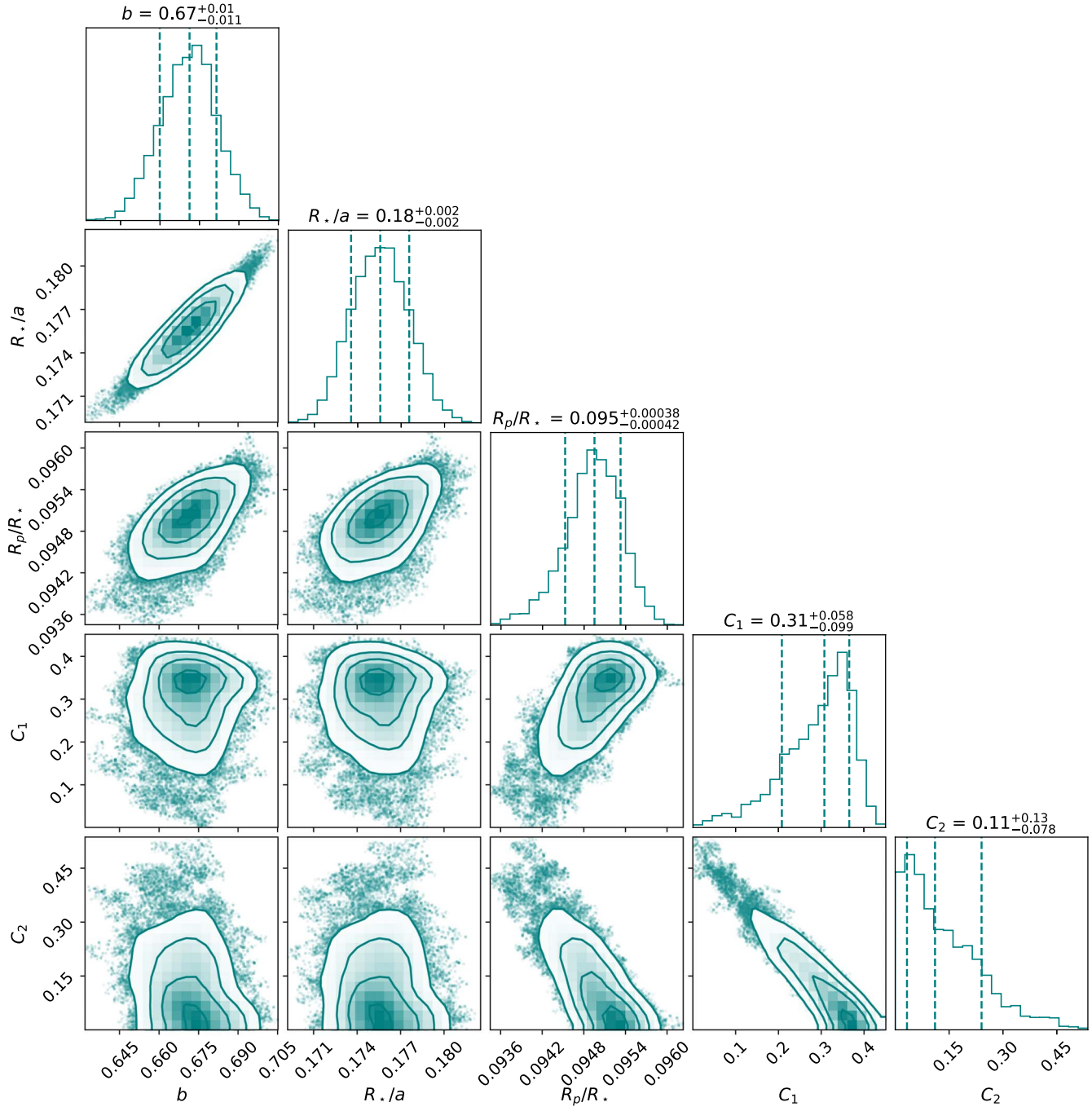

Figure 7. Corner plot showing the posterior distribution of the directly estimated transit parameters from the MCMC sampling for KELT-3 b.

provides an essential edge to the present study, as the accuracy of the estimated parameters can be considered higher than the previous studies involving only ground-based observations.

The next factor that affects the estimated parameters, including the studies involving space-based observations, is the unidentified noise components in the observational data. Even the extremely high-S/N data sets from space-based observations contain correlated noise components originating from short-term stellar variability, stellar activities, and pulsations. If untreated, these noise components can contribute to inaccurate estimation of the physical parameters, although precision may be high owing to the high-S/N data. In the present study, the previous proven and generally accepted GP regression technique has been used to efficiently model the correlated noise components in the transit lightcurves that model for the transit signal. This reduces the effect of these noise components in the estimated parameters from modeling, thus making them more accurate. Since almost all the previous studies of the target exoplanets studied in this work have not adopted any kind of correlated noise-treatment technique, the estimated parameters from this work can be treated as more accurate.

Another major factor contributing to the inaccurate estimation of physical properties is insufficient data sets. A single lightcurve could contain unidentifiable noise components, which could be treated as a part of the transit signal while modeling the lightcurve. This will contribute to

Table 10
Comparison of Estimated Parameters with the Previous Studies Involving Observations from Spitzer, HST, Kepler, CHEOPS, and TESS

Target	Study	Instrument	b	$R_p/R_\star$	$a/R_\star$
KELT-11 b	This work		$0.437^{+0.071}_{-0.093}$	0.04644 ± 0.00051	$4.89^{+0.2}_{-0.19}$
	Beatty et al. (2017)	Spitzer	$0.404^{+0.013}_{-0.018}$	$0.0514^{+0.0032}_{-0.0038}$	4.98 ± 0.05
	Patel & Espinoza (2022)	TESS	$0.541^{+0.044}_{-0.061}$	0.0475 ± 0.0006	$4.61^{+0.18}_{-0.15}$
	Hord et al. (2021)	TESS	0.488 ± 0.074	0.04725 ± 0.00066	...
KELT-17 b	This work		0.586 ± 0.01	$0.09174^{+0.00028}_{-0.00031}$	$6.302^{+0.049}_{-0.051}$
	Garai et al. (2022)	CHEOPS, TESS	0.587 ± 0.011	0.0921 ± 0.0011	6.246 ± 0.077
KELT-19 A b	This work		$0.382^{+0.066}_{-0.085}$	$0.09645^{+0.00092}_{-0.00083}$	8.65 ± 0.26
	Garai et al. (2022)	CHEOPS, TESS	0.499 ± 0.018	0.0985 ± 0.001	8.213 ± 0.088
	Hord et al. (2021)	TESS	0.367 ± 0.106	0.09649 ± 0.00115	...
KELT-20 b	This work		$0.5193^{+0.006}_{-0.0058}$	$0.1157^{+0.00016}_{-0.00017}$	$7.447^{+0.027}_{-0.028}$
	Patel & Espinoza (2022)	TESS	$0.502^{+0.017}_{-0.016}$	0.1157 ± 0.0005	$7.53^{+0.06}_{-0.07}$
KELT-24 b	This work		$0.096^{+0.053}_{-0.059}$	$0.087^{+0.00013}_{-0.00011}$	$10.689^{+0.039}_{-0.066}$
	Maciejewski (2020)	TESS	...	$0.0901^{+0.0003}_{-0.0004}$	$7.89^{+0.14}_{-0.12}$
	Patel & Espinoza (2022)	TESS	$0.135^{+0.06}_{-0.076}$	$0.0871^{+0.0003}_{-0.0002}$	$9.97^{+0.07}_{-0.09}$
HAT-P-1 b	This work		$0.733^{+0.021}_{-0.029}$	$0.1161^{+0.0013}_{-0.0015}$	$10^{+0.28}_{-0.27}$
	Nikolov et al. (2014)	HST	$0.7501^{+0.0064}_{-0.0069}$	0.11802 ± 0.00018	9.853 ± 0.071
HAT-P-2 b	This work		$0.456^{+0.027}_{-0.034}$	$0.06967^{+0.00026}_{-0.00031}$	$9.76^{+0.17}_{-0.14}$
	Patel & Espinoza (2022)	TESS	$0.457^{+0.035}_{-0.04}$	0.0691 ± 0.0004	$9.04^{+0.19}_{-0.18}$
HAT-P-11 b	This work		$0.107^{+0.071}_{-0.081}$	$0.05885^{+0.00024}_{-0.0003}$	$16.756^{+0.098}_{-0.154}$
	Sanchis-Ojeda & Winn (2011)	Kepler	0.132 ± 0.045	0.05862 ± 0.00026	15.6 ± 1.5
HAT-P-69 b	This work		$0.23^{+0.12}_{-0.16}$	$0.08453^{+0.00073}_{-0.0007}$	$7.74^{+0.17}_{-0.27}$
	Zhou et al. (2019)	TESS	$0.366^{+0.06}_{-0.05}$	$0.08703^{+0.00075}_{-0.0008}$	$7.32^{+0.16}_{-0.18}$
	Patel & Espinoza (2022)	TESS	$0.26^{+0.1}_{-0.15}$	$0.0849^{+0.0009}_{-0.0008}$	$7.68^{+0.19}_{-0.25}$
	Hord et al. (2021)	TESS	0.463 ± 0.27	0.0865 ± 0.0121	...
HAT-P-70 b	This work		$0.554^{+0.03}_{-0.043}$	$0.0924^{+0.00075}_{-0.00088}$	$5.44^{+0.15}_{-0.12}$
	Zhou et al. (2019)	TESS	$0.629^{+0.081}_{-0.054}$	$0.09887^{+0.00133}_{-0.00095}$	$5.45^{+0.29}_{-0.49}$
	Patel & Espinoza (2022)	TESS	$0.543^{+0.028}_{-0.032}$	$0.093^{+0.0008}_{-0.0009}$	$5.52^{+0.12}_{-0.11}$
	Hord et al. (2021)	TESS	0.464 ± 0.267	0.08712 ± 0.01055	...
XO-3 b	This work		$0.694^{+0.027}_{-0.029}$	$0.08826^{+0.00075}_{-0.00069}$	$6.99^{+0.22}_{-0.21}$
	Wong et al. (2014)	Spitzer	...	0.08825 ± 0.00037	$7.052^{+0.076}_{-0.097}$
	Patel & Espinoza (2022)	TESS	$0.696^{+0.028}_{-0.033}$	0.0888 ± 0.0011	$7.09^{+0.24}_{-0.23}$
WASP-7 b	This work		$0.532^{+0.046}_{-0.049}$	$0.07892^{+0.00063}_{-0.00065}$	$9.17^{+0.29}_{-0.3}$
	Patel & Espinoza (2022)	TESS	$0.53^{+0.038}_{-0.05}$	$0.079^{+0.0007}_{-0.0006}$	$8.93^{+0.29}_{-0.25}$
WASP-8 b	This work		0.64 ± 0.018	$0.11747^{+0.00087}_{-0.00102}$	$12.87^{+0.19}_{-0.21}$
	Hord et al. (2021)	TESS	0.601 ± 0.026	0.11925 ± 0.00181	...
WASP-14 b	This work		$0.545^{+0.033}_{-0.052}$	$0.09435^{+0.00083}_{-0.00121}$	$5.78^{+0.18}_{-0.13}$
	Wong et al. (2015)	Spitzer	...	0.09419 ± 0.00043	5.99 ± 0.09
WASP-18 b	This work		$0.395^{+0.019}_{-0.022}$	$0.09836^{+0.0003}_{-0.00032}$	$3.44^{+0.028}_{-0.025}$
	Cortés-Zuleta et al. (2020)	TESS	$0.36^{+0.11}_{-0.18}$	0.1018 ± 0.0011	$3.48^{+0.16}_{-0.17}$
WASP-33 b	This work		$0.06^{0.065}_{-0.04}$	$0.11036^{+0.00071}_{-0.00064}$	$3.6716^{+0.0093}_{-0.0175}$
	von Essen et al. (2020)	TESS	...	0.10716 ± 0.00023	3.605 ± 0.009
WASP-99 b	This work		$0.109^{+0.077}_{-0.069}$	$0.06774^{+0.00024}_{-0.00022}$	$8.691^{+0.049}_{-0.093}$
	Patel & Espinoza (2022)	TESS	$0.1^{+0.085}_{-0.065}$	0.0678 ± 0.0003	$8.71^{+0.04}_{-0.1}$
	Hord et al. (2021)	TESS	0.202 ± 0.118	0.06851 ± 0.00058	...
WASP-136 b	This work		$0.331^{+0.078}_{-0.103}$	$0.0683^{+0.00051}_{-0.00052}$	$7.31^{+0.22}_{-0.24}$
	Patel & Espinoza (2022)	TESS	$0.344^{+0.080}_{-0.121}$	0.0682 ± 0.0008	$7.31^{+0.26}_{-0.25}$
WASP-166 b	This work		$0.129^{+0.09}_{-0.085}$	$0.05158^{+0.0004}_{-0.00041}$	$11.99^{+0.15}_{-0.13}$
	Patel & Espinoza (2022)	TESS	$0.365^{+0.104}_{-0.089}$	0.0517 ± 0.0009	$11.25^{+0.38}_{-0.52}$
WASP-178 b	This work		$0.514^{+0.035}_{-0.045}$	$0.1068^{+0.00092}_{-0.0012}$	$7.2^{+0.17}_{-0.15}$
	Rodríguez Martínez et al. (2020)	TESS	$0.628^{+0.027}_{-0.029}$	$0.11066^{+0.0009}_{-0.00087}$	6.49 ± 0.18
	Hord et al. (2021)	TESS	0.433 ± 0.253	0.10538 ± 0.0107	...
WASP-189 b	This work		$0.358^{+0.047}_{-0.052}$	0.06984 ± 0.00032	$4.582^{+0.03}_{-0.037}$
	Lendl et al. (2020)	CHEOPS	$0.478^{+0.009}_{-0.012}$	$0.07045^{+0.00013}_{-0.00015}$	$4.6^{+0.031}_{-0.025}$

inaccurate estimation of the physical properties. A similar issue can also occur while using multiple but incomplete transit observations. By using multiple full-transit observations, such bias in modeling the transit signal can be overcome, resulting in more accurate parameter estimation. Some of the previous studies of the target exoplanets in this work, including some of the past studies involving TESS data, have used very limited data sets, which could have contributed to some bias in the estimated parameters. On the other hand, the present study has used extensive data sets from TESS observations covering a

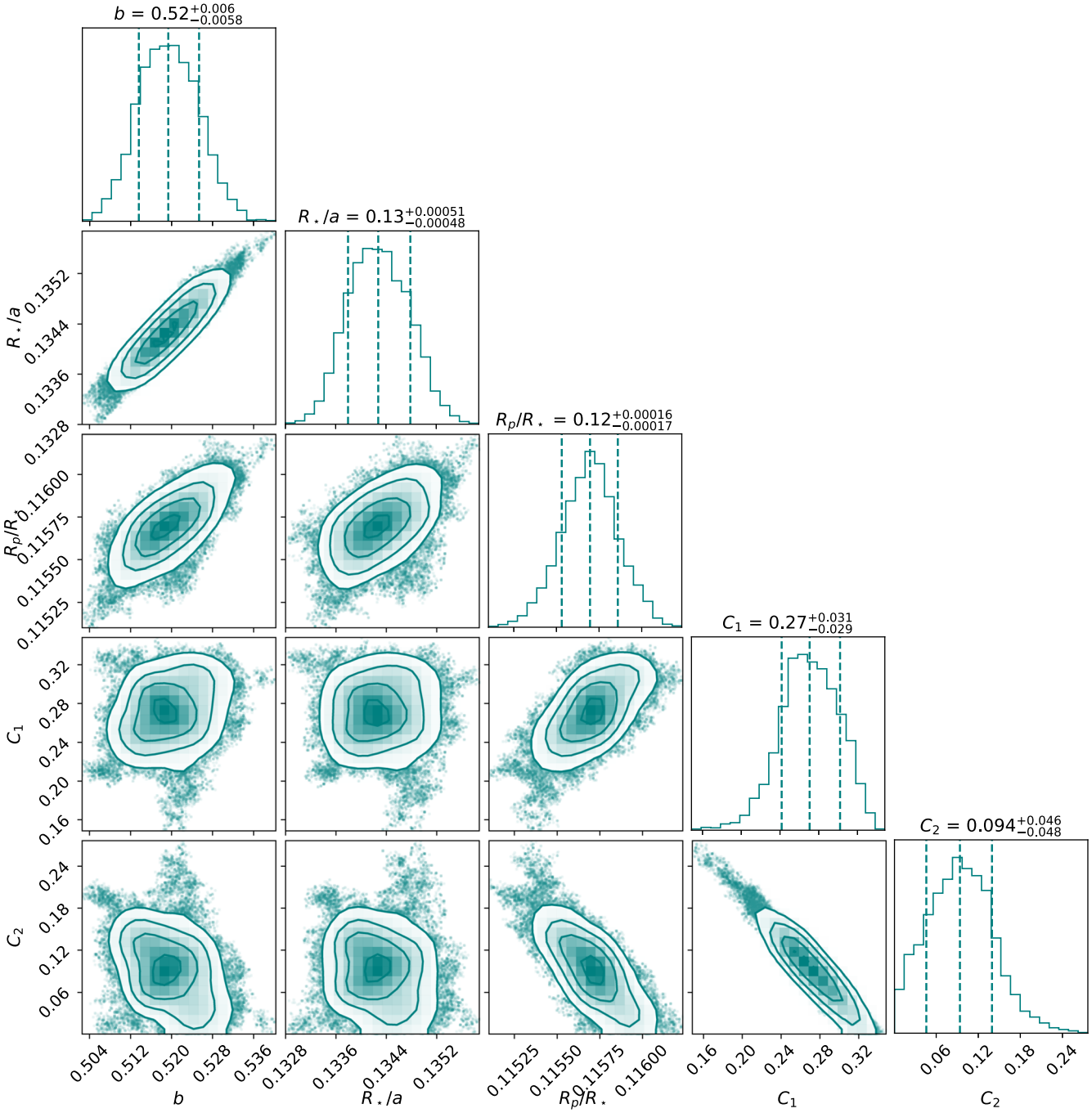

Figure 8. Same as Figure 7, but for KELT-20 b.

decent number of full-transit observations for each of the target exoplanets, which is expected to have minimized such bias in the estimated properties.

Apart from the above factors, the wavelength-dependent parameters, such as $R_p/R_\star$, would vary between studies depending upon the wavelength range of the photometric observations. In such cases, where the previous studies involve observations from a different space-based telescope, such as Spitzer, HST, or CHEOPS, the estimated values for $R_p/R_\star$ can be considered as complementary to the previously known values, thereby providing the scope for future multiwavelength studies to characterize the planetary atmospheres.

Summarizing the above discussions, the estimated transit parameters for the target exoplanets resulting from this work can be treated as extremely accurate and precise, and compared to the previous studies of these exoplanets, they can be regarded as the updated parameter values for most of the cases.

The other dependent physical properties, which were derived using the directly estimated transit parameters and the stellar properties adopted from the literature, also showed similar trends in improvements in their estimated values, as compared to the previous studies, which is expected. As a result, these parameter values are also extremely accurate and precise, and as such, can be regarded as the updated physical properties for the target exoplanets for most of the cases.

The orbital period, P, is not estimated directly from transit modeling of the lightcurves, but from the estimated midtransit

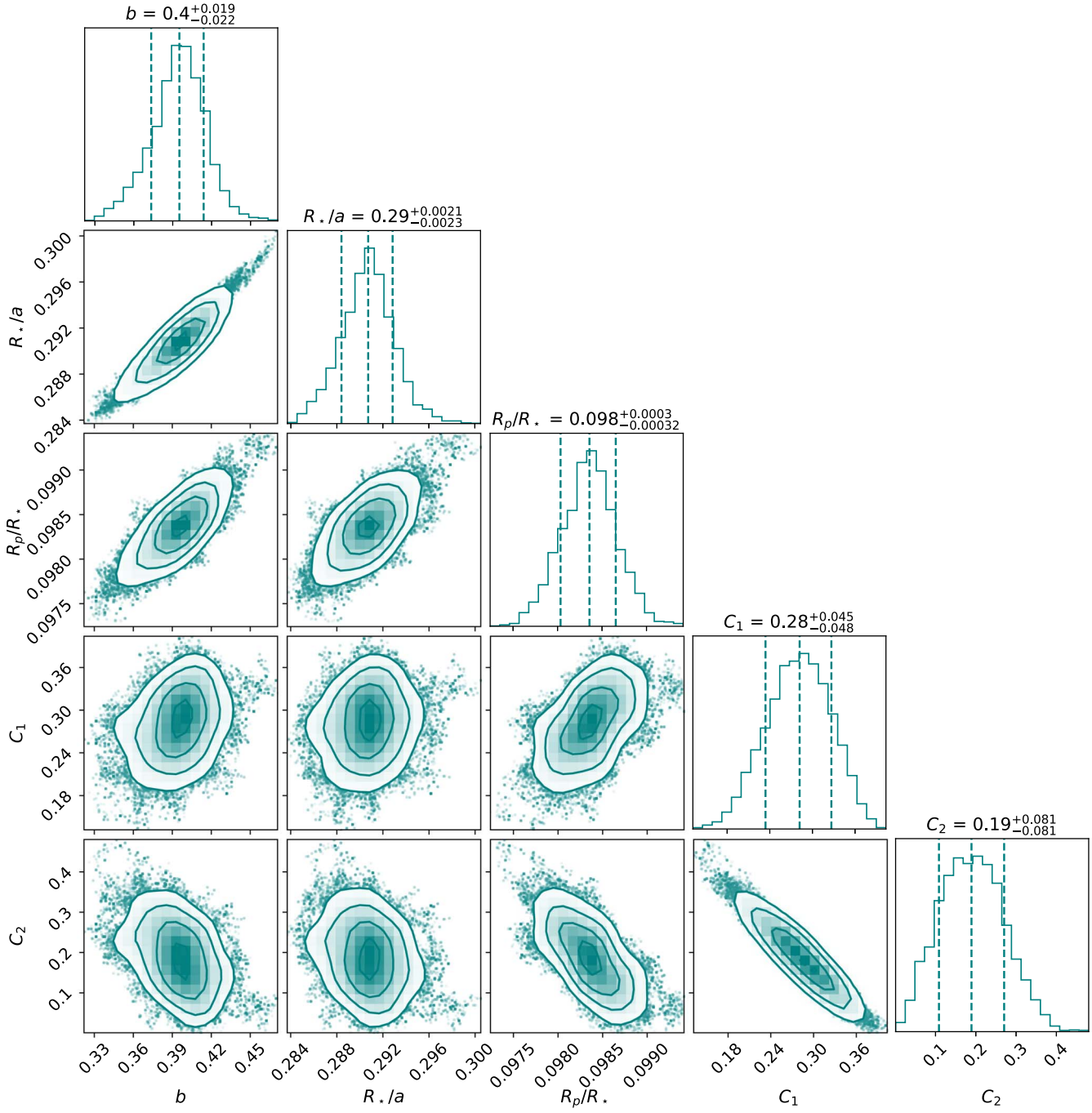

Figure 9. Same as Figure 7, but for WASP-18 b.

times. P depends upon the total span of time over which the transit observations have been conducted. Since I have only used the TESS transit photometric observations of the target exoplanets in this study, depending upon the span of the period over which the TESS data is available, the precision in the estimated value of P can vary significantly for each of the cases. For the cases where the target has been observed only in a single sector or a few consecutive sectors, the precision for P is comparatively less irrespective of the number of transits observed over that period. However, for the cases where the target has been observed in at least two sectors separated by a large timescale, the precision in the estimated values of P are very high. Compared with the previous studies, the precision in the estimated values of P from this study are higher for KELT-20 b, KELT-24 b, and WASP-76 b, and almost similar for KELT-2 A b, KELT-3 b, MASCARA-4 b, WASP-99 b, and WASP-166 b. For other cases, the precision in the estimated values of P were less compared to at least one of the previous studies, which can be attributed to the shorter total time span of TESS observations as discussed above. However, with more TESS observations of these targets in future sectors, P can be estimated more precisely.

Other than the planetary properties, the quadratic limb-darkening coefficients for the host stars were also estimated precisely while modeling the transit lightcurves. They are given along with the planetary properties in Tables 2–8. The best-fit

GP regression model parameters for each of the targets are given in Table 9.

The major output from this study has been the updated physical properties of 28 transiting exoplanets orbiting around bright stars with $V_{\rm mag} \leqslant 10$. These updated parameter values, as discussed above, are more precise for most of the cases compared to the previous studies, as well as more accurate and reliable. In the present era of large-scale studies in the field of exoplanet science, these updated values of physical properties of several known exoplanets would be immensely useful in a plethora of different studies, starting from the studies of planetary evolution and dynamics (e.g., Boley et al. 2020; Petrovich et al. 2020; Hamer & Schlaufman 2022; Rozner et al. 2022; Vissapragada et al. 2022), to their compositional studies (e.g., O'Neill et al. 2020; Berardo & de Wit 2022; Edwards & Tinetti 2022; Spaargaren et al. 2023), and the search for planetary companions, such as exomoons (e.g., Forgan & Kipping 2013; Trani et al. 2020; Saha & Sengupta 2022; Tokadjian & Piro 2023), etc. This study also demonstrates how large-scale survey missions of future can shape our understanding of existing planetary populations even further.

Acknowledgments

I thank the Scientific Editor for the valuable suggestions in improving the manuscript. I thank the anonymous reviewer for the valuable comments and suggestions. Some of the computational results reported in this work were performed on the high-performance computing facility (NOVA) of IIA, Bangalore. I am thankful to the computer division of the Indian Institute of Astrophysics for the help and cooperation extended to us. This paper includes data collected by the TESS mission, which are publicly available from the Mikulski Archive for Space Telescopes (MAST). I acknowledge the use of public TOI release data from pipelines at the TESS Science Office and at the TESS Science Processing Operations Center. Funding for the TESS mission is provided by NASA's Science Mission directorate. Support for MAST is provided by the NASA Office of Space Science via grant NNX13AC07G and by other grants and contracts. This research made use of Lightkurve, a Python package for Kepler and TESS data analysis.

ORCID iDs

Suman Saha https://orcid.org/0000-0001-8018-0264

References

Barros, S. C. C., Demangeon, O., Díaz, R. F., et al. 2020, A&A, 634, A75
Beatty, T. G., Pepper, J., Siverd, R. J., et al. 2012, ApJL, 756, L39
Beatty, T. G., Stevens, D. J., Collins, K. A., et al. 2017, AJ, 154, 25
Berardo, D., & de Wit, J. 2022, ApJ, 941, 155
Boley, A. C., Van Laerhoven, C., & Granados Contreras, A. P. 2020, AJ, 159, 207
Bonomo, A. S., Desidera, S., Benatti, S., et al. 2017, A&A, 602, A107
Chakrabarty, A., & Sengupta, S. 2019, AJ, 158, 39
Cortés-Zuleta, P., Rojo, P., Wang, S., et al. 2020, A&A, 636, A98
Daubechies, I. 1988, Commun. Pure Appl. Math., 41, 909
Daubechies, I. 1992, Ten Lectures on Wavelets (Philadelphia, PA: SIAM)
Donoho, D., & Johnstone, I. 1994, CRASM, 319, 1317
Dorval, P., Talens, G. J. J., Otten, G. P. P. L., et al. 2020, A&A, 635, A60
Eastman, J. D., Beatty, T. G., Siverd, R. J., et al. 2016, AJ, 151, 45
Edwards, B., & Tinetti, G. 2022, AJ, 164, 15
Forgan, D., & Kipping, D. 2013, MNRAS, 432, 2994
Garai, Z., Pribulla, T., Kovács, J., et al. 2022, MNRAS, 513, 2822
Hamer, J. H., & Schlaufman, K. C. 2022, AJ, 164, 26
Hastings, W. 1970, Biometrika, 57, 97
Hellier, C., Anderson, D. R., Barkaoui, K., et al. 2019a, MNRAS, 490, 1479
Hellier, C., Anderson, D. R., Collier Cameron, A., et al. 2014, MNRAS, 440, 1982
Hellier, C., Anderson, D. R., Triaud, A. H. M. J., et al. 2019b, MNRAS, 488, 3067
Hjorth, M., Albrecht, S., Talens, G. J. J., et al. 2019, A&A, 631, A76
Hord, B. J., Colón, K. D., Kostov, V., et al. 2021, AJ, 162, 263
Jenkins, J. M. 2017, Kepler Data Processing Handbook: Overview of the Science Operations Center, Kepler Science Document, KSCI-19081-002
Johnson, M. C., Cochran, W. D., Collier Cameron, A., & Bayliss, D. 2015, ApJL, 810, L23
Knutson, H. A., Fulton, B. J., Montet, B. T., et al. 2014, ApJ, 785, 126
Lam, K. W. F., Faedi, F., Brown, D. J. A., et al. 2017, A&A, 599, A3
Lee, G. R., Gommers, R., Waselewski, F., Wohlfahrt, K., & O'Leary, A. 2019, JOSS, 4, 1237
Lehmann, H., Guenther, E., Sebastian, D., et al. 2015, A&A, 578, L4
Lendl, M., Csizmadia, S., Deline, A., et al. 2020, A&A, 643, A94
Lund, M. B., Rodriguez, J. E., Zhou, G., et al. 2017, AJ, 154, 194
Luo, G., & Zhang, D. 2012, in Advances in Wavelet Theory and their Applications in Engineering, Physics and Technology, ed. D. Baleanu (Rijeka: IntechOpen), 59
Maciejewski, G. 2020, AcA, 70, 181
Mancini, L., Esposito, M., Covino, E., et al. 2018, A&A, 613, A41
Mandel, K., & Agol, E. 2002, ApJL, 580, L171
Ment, K., Fischer, D. A., Bakos, G., Howard, A. W., & Isaacson, H. 2018, AJ, 156, 213
Nikolov, N., Sing, D. K., Pont, F., et al. 2014, MNRAS, 437, 46
O'Neill, C., Lowman, J., & Wasiliev, J. 2020, Icar, 352, 114025
Pan, Q., Zhang, L., Dai, G., & Zhang, H. 1999, ITSP, 47, 3401
Patel, J. A., & Espinoza, N. 2022, AJ, 163, 228
Pepper, J., Rodriguez, J. E., Collins, K. A., et al. 2017, AJ, 153, 215
Pepper, J., Siverd, R. J., Beatty, T. G., et al. 2013, ApJ, 773, 64
Pereira, F., Campante, T. L., Cunha, M. S., et al. 2019, MNRAS, 489, 5764
Petrovich, C., Muñoz, D. J., Kratter, K. M., & Malhotra, R. 2020, ApJL, 902, L5
Rasmussen, C. E., & Williams, C. K. I. 2006, Gaussian Processes for Machine Learning (Cambridge, MA: MIT Press)
Ricker, G. R., Winn, J. N., Vanderspek, R., et al. 2015, JATIS, 1, 014003
Rodriguez, J. E., Eastman, J. D., Zhou, G., et al. 2019, AJ, 158, 197
Rodríguez Martínez, R., Gaudi, B. S., Rodriguez, J. E., et al. 2020, AJ, 160, 111
Rowe, A. C. H., & Abbott, P. C. 1995, ComPh, 9, 635
Rozner, M., Glanz, H., Perets, H. B., & Grishin, E. 2022, ApJ, 931, 10
Saha, S., Chakrabarty, A., & Sengupta, S. 2021, AJ, 162, 18
Saha, S., & Sengupta, S. 2021, AJ, 162, 221
Saha, S., & Sengupta, S. 2022, ApJ, 936, 2
Sanchis-Ojeda, R., & Winn, J. N. 2011, ApJ, 743, 61
Siverd, R. J., Collins, K. A., Zhou, G., et al. 2018, AJ, 155, 35
Smith, J. C., Stumpe, M. C., Cleve, J. E. V., et al. 2012, PASP, 124, 1000
Southworth, J. 2012, MNRAS, 426, 1291
Spaargaren, R. J., Wang, H. S., Mojzsis, S. J., Ballmer, M. D., & Tackley, P. J. 2023, ApJ, 948, 53
Stassun, K. G., Collins, K. A., & Gaudi, B. S. 2017, AJ, 153, 136
Stassun, K. G., Oelkers, R. J., Paegert, M., et al. 2019, AJ, 158, 138
Stumpe, M. C., Smith, J. C., Catanzarite, J. H., et al. 2014, PASP, 126, 100
Stumpe, M. C., Smith, J. C., Van Cleve, J. E., et al. 2012, PASP, 124, 985
Talens, G. J. J., Justesen, A. B., Albrecht, S., et al. 2018, A&A, 612, A57
Tokadjian, A., & Piro, A. L. 2023, AJ, 165, 173
Trani, A. A., Hamers, A. S., Geller, A., & Spera, M. 2020, MNRAS, 499, 4195
Tsantaki, M., Sousa, S. G., Santos, N. C., et al. 2014, A&A, 570, A80
Vissapragada, S., Chontos, A., Greklek-McKeon, M., et al. 2022, ApJL, 941, L31
von Essen, C., Mallonn, M., Borre, C. C., et al. 2020, A&A, 639, A34
West, R. G., Hellier, C., Almenara, J. M., et al. 2016, A&A, 585, A126
Wong, I., Knutson, H. A., Cowan, N. B., et al. 2014, ApJ, 794, 134
Wong, I., Knutson, H. A., Lewis, N. K., et al. 2015, ApJ, 811, 122
Yee, S. W., Petigura, E. A., Fulton, B. J., et al. 2018, AJ, 155, 255
Zhou, G., Huang, C. X., Bakos, G. Á., et al. 2019, AJ, 158, 141
Zhou, G., Rodriguez, J. E., Collins, K. A., et al. 2016, AJ, 152, 136